Journal of Theoretical Biology 547 (2022) 111135

Contents lists available at ScienceDirect

Journal of Theoretical Biology

journal homepage: www.elsevier.com/locate/yjtbi

Spreading speed of chronic wasting disease across deer groups with overlapping home ranges

Jingjing Xu [a,b,*], Evelyn H. Merrill [b], Mark A. Lewis [a,b]

[a] Department of Mathematical and Statistical Sciences, University of Alberta, 116 St. and 85 Ave., Edmonton, AB T6G 2R3, Canada
[b] Department of Biological Science, University of Alberta, 116 St. and 85 Ave., Edmonton, AB T6G 2R3, Canada

ARTICLE INFO

Article history:
Received 6 July 2021
Revised 13 April 2022
Accepted 17 April 2022
Available online 28 April 2022

Keywords:
Differential equations
Restricted movement
Landscape heterogeneity
Chronic wasting disease
Spreading speed

ABSTRACT

Chronic wasting disease (CWD) is a fatal disease of cervid species that continues to spread across North America and now in Europe. It poses a threat to cervid populations and the local ecological and economic communities that depend on them. Although empirical studies have shown that host home range overlap and male dispersal are important in the spread of disease, there are few mechanistic models explicitly considering those factors. We built a spatio-temporal, differential equation model for CWD spreading with restricted movement of hosts within home ranges. The model incorporates both direct and environmental transmission within and between groups as well as male dispersal. We compared the relative influence of host density, sex ratio, home range size, and male dispersal distance on the spreading speed using sensitivity analysis. We also assessed the effect of landscape heterogeneity, quantified as edge density, on the spreading speed of CWD because it jointly alters the host density and home range size. Our model binds the theoretical study of CWD spreading speed together with empirical studies on deer home ranges and sets a base for models in 2D space to evaluate management and control strategies.

1. Introduction

Chronic wasting disease (CWD) is a prion-based transmissible spongiform encephalopath in deer species (cervids) that leads to a 100% mortality (EFSA BIOHAZ Panel, 2017). The disease is spread from individual to individual (direct transmission) but also through the environment (indirect transmission) due to the persistence of excreted prions from saliva, blood, urine, and carcass of infected hosts (Williams et al., 2002; Williams, 2005; Mathiason et al., 2006). The latent period of CWD is one to two years, but even during this period, animals can be contagious and shed prions into the environment. Populations are expected to decline by 10–21% when prevalence exceeds 30% in deer species (*Odocoileus* spp.) (Edmunds et al., 2016; DeVivo et al., 2017) and elk (*Cervus* spp.) population starts to decline with a prevalence of 13% (Monello et al., 2014). Widespread loss of cervid populations will result in economic loss to local communities from diminished hunting and tourism, and could result in major ecological changes influencing the conservation of biodiversity (Rivera et al., 2019; Escobar et al., 2020). Because no vaccine is available, management options for controlling the spread of CWD remain limited with most focused on non-selective harvesting targeting males, or removals of individuals associated with locations of known CWD-infected individuals (Uehlinger et al., 2016; Mysterud and Rolandsen, 2018; Rivera et al., 2019). The disease continues to spread and is now reported in free-ranging cervids in 28 states in the USA and three Canadian provinces (USGS, updated March, 2022), as well as in isolated areas in Norway, Sweden and Finland. Understanding which factors play a key role in the speed at which CWD spreads is important in directing current and future management strategies to control or contain the disease.

Previous approaches to model the spread of CWD have ranged from statistical models based on regression and spatial clustering analyses to models with detailed mechanisms of disease transmission. Spatially explicit, statistical models estimate risk based on associated factors such as host type and landscape features (O'Hara Ruiz et al., 2013; Robinson et al., 2013), and provide valuable information to direct surveillance and management (Nobert et al., 2016), but typically do not lend themselves to making predictions over time. For this reason, mechanistic models that include the mechanisms of disease transmission over changing conditions, are particularly powerful in the prediction of CWD spread (Michael, 2001; Garlick et al., 2014; Hefley et al., 2017). Mechanistic models include individual-based models and mathematical/epidemiological models. Individual-based models can provide more mechanistic realism, such as social grouping dynamics,

* Corresponding author at: Department of Mathematical and Statistical Sciences, University of Alberta, 116 St. and 85 Ave., Edmonton, AB T6G 2R3, Canada.
E-mail address: ji9@ualberta.ca (J. Xu).

https://doi.org/10.1016/j.jtbi.2022.111135
0022-5193/

with the flexibility to deal with landscape heterogeneity, spatial structure, and adaptation (Hammond, 2015), but have high data and computational requirements (Hammond, 2015; Michael, 2001; Belsare et al., 2020). Epidemiological models that include population-level dynamics and disease transmission are useful to assess direct hypotheses about key factors influencing the rate of disease spread, and may uncover the possible critical factors in the transmission routes at scales ranging from local to regional (Potapov et al., 2012; Potapov et al., 2013; Potapov et al., 2016). For example, Garlick et al. (2014) introduced an averaging method to efficiently estimate CWD spreading speed in a state scale, based on population size and ecological diffusion of deer in heterogeneous landscapes. Hefley et al. (2017) incorporated the ecological diffusion into a Bayesian framework to address disease spread, and found that incorporating a more mechanistic framework into statistical model outperformed regression and machine learning approaches. However, these models ignored the fact that a good portion of deer live in groups, which leads to a higher contact rate among members of the same group than the contact rate of a pair of deer from different groups (Merrill et al., 2011).

We use an alternative mechanistic framework that is based on overlapping home ranges to assess the importance of factors influencing CWD spreading speed. A model using home range on lattices to address ecological processes was first introduced in 1971 by Holgate (1971), and extended to continuous space by Lewis et al. (1997) and Moorcroft (1997). Since then, mechanistic home range models have been widely used to study animal movement and pattern formation of territories (Lewis and Murray, 1993; Moorcroft et al., 1999; Briscoe et al., 2002; Hamelin and Lewis, 2010; Auger-Méthé et al., 2016). To our knowledge, Reluga et al. (2006) first introduced the approach to addressing theoretical disease spread. We adopt Reluga et al. (2006)'s restricted-movement model into the CWD spreading model, incorporating both direct and environmental transmission within a group and between groups as well as male dispersal.

Landscape heterogeneity has been shown to affect deer movement and their home ranges at multiple scales (Adams et al., 2020; Kie et al., 2002), which affects the encounter rate, and hence, the spread of CWD, but very few models for CWD have incorporated home-range structure. Our work builds a bridge between the empirical studies and mechanistic home-range models that can be used to examine the relationships between landscape heterogeneity and disease spread. For example, deer are reported to respond to woody-cover edge (i.e., the border between woody cover and other vegetation types) in multiple ways. Edges are preferred vegetation because they provide a diversity of forages and thermal cover in close proximity and protection from predation (Massé et al., 2009; Altendorf et al., 2001; D. Freddy et al., 1985; Cook et al., 2004). In landscape ecology, edges are the boundaries between different vegetation types, and *edge density* equals the edge length per unit area (e.g., km/km^2; see Appendix J, also). Higher edge density is correlated with smaller home ranges, and also supports a larger deer density (Adams et al., 2020; Walter et al., 2018; Plante et al., 2004), both of which may be associated with disease spread (Habib et al., 2011). Including the home range structure and the effects of landscape features on home range sizes offers an opportunity to make use of data from empirical studies and provides a means of identifying areas with higher spread potentials and evaluating management or control strategies for CWD through manipulating edges.

In this paper, we present a CWD spread framework that is based on a spatio-temporal system of coupled differential equations and incorporates a home-range structure (Reluga et al., 2006; Moorcroft et al., 2006) and dispersal across home ranges. In our model, deer share space with the members of their group, so the within-group space use influences within-group contact; deer from different groups may have overlapping home ranges, which determines the frequency of between-group contact. Infectious hosts spread the disease by direct contact or by shedding the prions to the environment, which hosts are exposed to within overlapping home ranges. By incorporating these features, we are able to project disease spread over relatively large spatial areas through both direct contacts with an infected individual (within a group or from another group) as well as exposure to prions through the environment.

Below we first present model components to build a one-dimensional framework (Fig. 1), followed by numerical simulations of spreading speed under a specific arrangement of groups, which inspires our derivation of a spreading speed formula for the disease. We deduce the spreading speed of the disease from the minimum possible traveling wave speed, based on a linearization about the leading edge of the spreading disease. We then illustrate the relative influence of host density, sex ratio, home range size, and male dispersal distance on the spreading speed using local sensitivity analysis, first when factors are assumed independent from each other; and second, when we simultaneously change host density and home range size by altering edge density. Finally, we describe an ongoing future work that extends this model to 2D space , which can enhance our understanding of the driving factors of CWD spread and assess various harvesting strategies.

2. Model

We construct a model based on grouping individuals within home ranges, with the dispersal of males between home ranges. We include disease transmission within and between groups and derive a system of coupled ordinary differential equations for the disease spread.

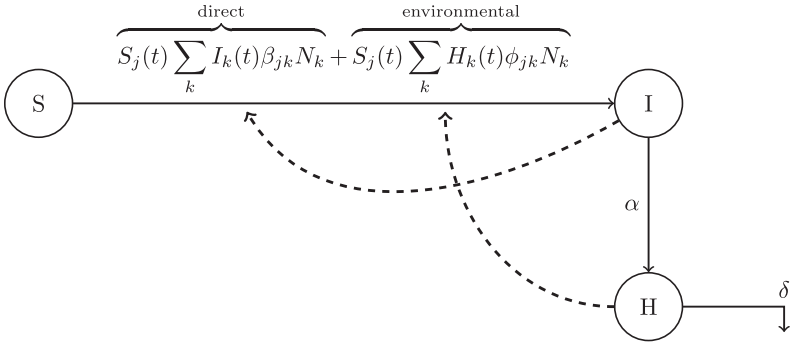

Fig. 1. An illustration of direct and environmental transmission between different components in the model. Male dispersal is not shown here.

2.1. Grouping structure and home ranges

We structure the population such that deer live in groups and that groups are distinguished as either male or female groups (Mejia Salazar et al., 2017). If we assume that there are an equal number of male groups and female groups, then it is possible to determine the number of individuals in a group from the deer density and population sex ratio in a simulation. This approach is used in simulations in Section 3. The number of deer in a group (i.e., the group size) is assumed to remain unchanged over time, a simplification reflecting the assumption of a stable population density. Groups are located discretely in one-dimensional space. Individuals in each group have a spatially distributed symmetric home range around a location, x_j (see Fig. 2), which creates the possibility of overlapping home ranges between groups. The probability distribution for spatial use by each individual in a group is given for each group, and the location of one home range does not influence another. Within home ranges, the probabilistic distribution in space is the same for all individuals in a group. It is assumed to result from two balancing processes: random motion and a directed motion towards a given location, i.e., the center of the home range (see Section 2.2). The frequency of pairwise interaction among individuals within the same group is then determined by the probabilistic distribution arising from these processes. The between-group pairwise interaction is determined by both the distance between the location of the home range centers and the probabilistic distribution of individuals within a home range.

2.2. Home range based on a restricted movement model

Restricted movement within a home range. Suppose a group of deer move around a center x_j, and the distribution of deer space use within a home range results from restricted movement, which includes a random motion with diffusion coefficient D and a directed motion towards the center with speed c (Reluga et al., 2006; Moorcroft et al., 2006). The steady state distribution of a deer group is

$$\bar{u}(x) = N u(x), \tag{1}$$

where N is the group size, and $u(x)$ is the probabilistic distribution of a deer in this group, with

$$u(x) = \frac{b}{2}\exp(-b|x - x_j|), \tag{2}$$

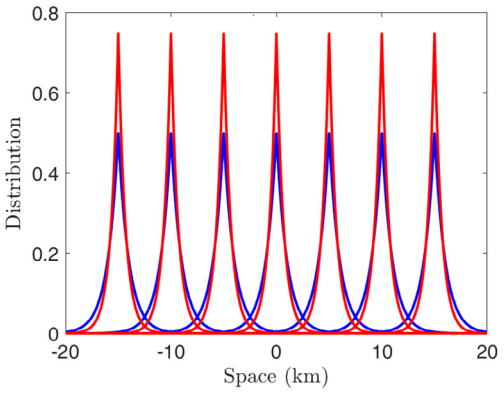

Fig. 2. Distribution of groups over space when we assume the same number of male and female groups. Red is for female group distribution, and blue for male. Here, there are seven female groups and seven male groups. Male groups are located around the same seven locations for female groups. The distance between neighbouring groups is set to $\Delta x = 5\ km$, and the home ranges are determined by $b_m = 1\,\mathrm{km^2 yr^{-1}}$, $b_f = 1.4979\,\mathrm{km^2 yr^{-1}}$.

where the relative strength of directed motion is $b = \frac{c}{D}$ (see Moorcroft et al., 2006, page 31).

When the relative strength of the directed motion b is unknown, it can be related to the size of the home range. The relationship between the parameter b and the radius of the 95% home range, r, comes from Eq. (2). We use the radius here in 1D to mean the distance from the home range center to the edge of 95% home range. A 95% home range corresponds to the relation

$$0.95 = \int_{-r}^{r} \frac{b}{2}\exp(-b|x|)dx, \tag{3}$$

which gives us

$$b = \frac{\ln(20)}{r}. \tag{4}$$

2.3. Direct and environmental transmission within and between groups

We assume that infectious hosts (I) spread the disease by direct contact with susceptible hosts (S) or by shedding the prions to the environment (H), which susceptible hosts (S) can pick up from overlapping home ranges (see Table 1 for notations, and Fig. 1).

We also assume there are multiple groups, each with a different home range location, so that group j is centered around home range center x_j. Based on the steady-state distribution, we derive a model for both sexes without considering dispersal (see Appendix A for derivations). We will consider male dispersal in the next section. The proportions of susceptible $S_j(t)$ and infected $I_j(t)$ hosts in group j, and the average group-j per-individual shedding amount of prions $H_j(t)$ (that is, the total prion amount shed by a size-N_j group is H_jN_j) obey the following ordinary differential equations (ODEs):

Table 1
Notations (s represents sex, f for female, m for male. In general cases for both sexes, we omit the s superscript in the notations.)

Notation	Description
F	the number of female groups
M	the number of male groups
N_s	the group size of sex s
x_j	center of home range for group j
Δx	distance between the centers of neighbouring groups
b_s	relative strength of directed motion compared with the random motion of sex s
c_1, c_2	parameters determining the male dispersal
β	the basic direct transmission rate
ϕ	the basic environmental transmission rate
α	the rate at which prions are excreted
δ	the degrading rate of prions from environment
$u_j^s(x)$	the probability density of group j of sex s
N_k^s	the number of individuals in group k of sex s
$S_j^s(t)$	the proportion of susceptible individuals in group j of sex s
$I_j^s(t)$	the proportion of infected individuals in group j of sex s
$H_j^s(t)$	the amount of prions shed from group j of sex s
β_{jk}^s	direct transmission rate from group k to group j of sex s
$\beta_{j\ell}^{xy}$	direct transmission rate from sex-y group ℓ to sex-x group j
ϕ_{jk}^{xy}	transmission rate from prions shed by sex-y group k to sex-x group j
ϕ_{jk}^s	transmission rate from prions shed by group k to group j for sex s
μ_{jk}	the coefficient of pairwise encounter rate
e_{jk}	the rate of male dispersal from group k to group j

$$\frac{d}{dt}S_j(t) = -S_j(t)\sum_k I_k(t)\beta_{jk}N_k - S_j(t)\sum_k H_k(t)\phi_{jk}N_k, \tag{5}$$

$$\frac{d}{dt}I_j(t) = S_j(t)\sum_k I_k(t)\beta_{jk}N_k + S_j(t)\sum_k H_k(t)\phi_{jk}N_k, \tag{6}$$

$$\frac{d}{dt}H_j(t) = \alpha I_j(t) - \delta H_j(t), \tag{7}$$

where

$$\beta_{jk} = \beta\mu_{jk}, \tag{8}$$

$$\phi_{jk} = \phi\mu_{jk}, \tag{9}$$

$$\mu_{jk} = \int_R u_j(\xi)u_k(\xi)d\xi, \tag{10}$$

where we call β_{jk} the coefficient of pairwise direct effective transmission, ϕ_{jk} the coefficient of pairwise environmental effective transmission, and μ_{jk} the pairwise encounter rate. Note that $j = k$ indicates transmission within a group, and $j \neq k$ indicates transmission between groups.

2.4. Dynamics of male groups with dispersal

In addition to the random motion and directed motion of individual group members within each home range, which is used to derive the steady-state distribution in Eq. (2), the male distribution among groups is modified via dispersal between groups. We use $N_j(t)$ to denote the number of deer in group j, and use e_{jk} to denote the rate at which males in group k disperse to group j. For M male groups, the change of group size is given by

$$\frac{d}{dt}N_j(t) = \sum_{k=1,k\neq j}^{M} e_{jk}N_k - \sum_{k=1,k\neq j}^{M} e_{kj}N_j. \tag{11}$$

The system can be written in the following matrix form,

$$\dot{\mathbf{N}}(t) = \mathbf{E}\mathbf{N}(t), \tag{12}$$

where

$$\mathbf{E} = \begin{bmatrix} -\sum_{k=1,k\neq 1}^{M} e_{k,1} & e_{1,2} & \cdots & e_{1,M} \\ e_{2,1} & -\sum_{k=1,k\neq 2}^{M} e_{k,2} & \cdots & e_{2,M} \\ \vdots & \vdots & \vdots & \vdots \\ e_{M,1} & e_{M,2} & \cdots & -\sum_{k=1,k\neq M}^{M} e_{k,M} \end{bmatrix}. \tag{13}$$

Note: $\sum_{k=1}^{M} E_{kj} = 0$ for $j = 1, 2, \ldots, M$ and $e_{jk} > 0$. The total number of males remains constant because

$$\sum_{j=1}^{M}\frac{d}{dt}N_j(t) = 0, \tag{14}$$

so $\sum_{j=1}^{M} N_j(t) = \sum_{j=1}^{M} N_j(0) = K$, where K is the total number of males.

If we divide the equations by K, the system (11)-(12) corresponds to a Continuous Time Markov Chain (CTMC) (see Appendix G). Because males can disperse between each pair of male groups and there are a finite number of groups, the system corresponds to an irreducible and finite CTMC, that is, a positive recurrent CTMC. Therefore, there exists an equilibrium solution $\mathbf{N}^*$ satisfying $\mathbf{E}\mathbf{N}^* = \mathbf{0}$ which is the limiting probability distribution (see Pishro-Nik et al., 2016, Section 11.3.2). Thus

$$\lim_{t\to+\infty} N_j(t) = N_j^*. \tag{15}$$

We assume the male distribution is at equilibrium and we drop $*$ in the following sections to simplify the notation. For the special case when the dispersal is symmetric between groups, i.e., $e_{jk} = e_{kj}$, we can verify the existence of a uniform equilibrium by substituting $\mathbf{N}^* = (\frac{K}{M}, \frac{K}{M}, \frac{K}{M}, \ldots, \frac{K}{M})$ into the system (12). That is, the number 0 is an eigenvalue of $\mathbf{E}$ with the corresponding eigenvector $(1, 1, 1, \cdots, 1)$. All other eigenvalues have negative real parts. This can be proved by the direct application of the Gershgorin circle theorem. That is to say, the spectral abscissa (i.e., the largest real part of the eigenvalues) of $\mathbf{E}$ is zero. Furthermore, with the given total number of males, the solution to $\mathbf{E}\mathbf{N} = \mathbf{0}$ is $\mathbf{N}^*$.

2.5. Full model in finite domain

Assuming there are M male groups and F female groups, we combine the transmission model (see Fig. 1) and male dispersal to obtain the full model as follows:

$$\begin{aligned}\frac{d}{dt}S_j^f(t) =& -S_j^f(t)\sum_{k=1}^{F}\left(I_k^f(t)\beta_{jk}^f + H_k^f(t)\phi_{jk}^f\right)N_k^f \\ & - S_j^f(t)\sum_{q=1}^{M}\left(I_q^m(t)\beta_{jq}^{fm} + H_q^m(t)\phi_{jq}^{fm}\right)N_q^m,\end{aligned} \tag{16}$$

$$\begin{aligned}\frac{d}{dt}I_j^f(t) =& S_j^f(t)\sum_{k=1}^{F}\left(I_k^f(t)\beta_{jk}^f + H_k^f(t)\phi_{jk}^f\right)N_k^f \\ & + S_j^f(t)\sum_{q=1}^{M}\left(I_q^m(t)\beta_{jq}^{fm} + H_q^m(t)\phi_{jq}^{fm}\right)N_q^m,\end{aligned} \tag{17}$$

$$\frac{d}{dt}H_j^f(t) = \alpha I_j^f(t) - \delta H_j^f(t), \tag{18}$$

$$\begin{aligned}\frac{d}{dt}S_p^m(t) =& -S_p^m(t)\sum_{k=1}^{F}\left(I_k^f(t)\beta_{pk}^{mf} + H_k^f(t)\phi_{pk}^{mf}\right)N_k^f \\ & - S_p^m(t)\sum_{q=1}^{M}\left(I_q^m(t)\beta_{pq}^{m} + H_q^m(t)\phi_{pq}^{m}\right)N_q^m \\ & + \sum_{q\neq p} e_{pq}S_q^m(t)N_q^m - S_p^m(t)N_p^m\sum_{q\neq p} e_{qp},\end{aligned} \tag{19}$$

$$\begin{aligned}\frac{d}{dt}I_p^m(t) =& S_p^m(t)\sum_{k=1}^{F}\left(I_k^f(t)\beta_{pk}^{mf} + H_k^f(t)\phi_{pk}^{mf}\right)N_k^f \\ & + S_p^m(t)\sum_{q=1}^{M}\left(I_q^m(t)\beta_{pq}^{m} + H_q^m(t)\phi_{pq}^{m}\right)N_q^m \\ & + \sum_{q\neq p} e_{pq}I_q^m(t)N_q^m - I_p^m(t)N_p^m\sum_{q\neq p} e_{qp},\end{aligned} \tag{20}$$

$$\frac{d}{dt}H_p^m(t) = \alpha I_p^m(t) - \delta H_p^m(t), \tag{21}$$

where superscripts f and m on variables denote the sex as described in Table 1,

$$j = 1, 2, \cdots, F, \tag{22}$$
$$p = 1, 2, \cdots, M, \tag{23}$$
$$\beta_{jq}^{fm} = \beta \mu_{jq}^{fm}, \tag{24}$$
$$\phi_{jq}^{fm} = \phi \mu_{jq}^{fm}, \tag{25}$$
$$\mu_{jq}^{fm} = \int_R u_j^f(\xi) u_q^m(\xi) d\xi, \tag{26}$$
$$\beta_{pk}^{mf} = \beta \mu_{pk}^{mf}, \tag{27}$$
$$\phi_{pk}^{mf} = \phi \mu_{pk}^{mf}, \tag{28}$$
$$\mu_{pk}^{mf} = \int_R u_p^m(\xi) u_k^f(\xi) d\xi, \tag{29}$$
$$\beta_{jk}^{s} = \beta \mu_{jk}^{s}, \tag{30}$$
$$\phi_{jk}^{s} = \phi \mu_{jk}^{s}, \tag{31}$$
$$\mu_{jk}^{s} = \int_R u_j^s(\xi) u_k^s(\xi) d\xi, \tag{32}$$
$$s = f, m. \tag{33}$$

with initial conditions:

$$S_j^f(0) = S_{j,0}^f, I_j^f(0) = I_{j,0}^f, H_j^f(0) = H_{j,0}^f, \text{ for } j = 1, 2, \cdots, F, \tag{34}$$
$$S_p^m(0) = S_{p,0}^m, I_p^m(0) = I_{p,0}^m, H_p^m(0) = H_{p,0}^m, \text{ for } p = 1, 2, \cdots, M. \tag{35}$$

For the male dispersal rate e_{qp}, we assume an exponentially decreasing rate function

$$e_{qp} = e_{pq} = c_1 \exp(-c_2 \Delta x |p - q|), \tag{36}$$

where c_1 denotes the magnitude and c_2 denotes the drop off with distance. Note that the rate of dispersing deer is the product of the per capita dispersal rate and the number of deer. When per capita dispersal rates are the same in both directions, the sizes of two deer groups can change if the groups begin with different sizes. However, the sizes of the two groups remain the same if they start with the same size, because they "exchange" the same number of deer per time unit. Although denoted distinctly by N_q^m, here we assume the male groups are of the same size, which is later simplified to N_m. We present a more general model in Appendix H, where we track the number of hosts in the group instead of their proportions allowing the group sizes to be different.

2.6. Model in the infinite domain

In the infinite domain, the indices for j and p run from $-\infty$ to ∞, i.e., they are integers $\mathbb{Z}$ (see Eqs. (16)-(21)). For male groups, we restrict ourselves to the case where the per capita dispersal rate matrix $\mathbf{E}$ is symmetric and we assume that male group sizes are at the uniform equilibrium in the infinite domain, $\mathbf{N}^*$. Similar to the existence of a uniform equilibrium solution in the finite domain, we substitute the uniform equilibrium solution in the infinite domain into the version of the system (12) expanded into the infinite domain. For a given group j, the movement to any other group k balances out with the movement from that group k, so the existence of the uniform equilibrium solution with respect to male dispersal is guaranteed. The initial conditions are as follows:

$$S_j^f(0) = S_{j,0}^f, I_j^f(0) = I_{j,0}^f, H_j^f(0) = H_{j,0}^f, \text{ for } j \in \mathbb{Z}, \tag{37}$$
$$S_p^m(0) = S_{p,0}^m, I_p^m(0) = I_{p,0}^m, H_p^m(0) = H_{p,0}^m, \text{ for } p \in \mathbb{Z}. \tag{38}$$

2.7. Equilibrium

Here, we calculate equilibrium solutions for the spatially uniform problem (where each node is identical). On the finite domain, when the male groups are of a constant size (i.e., $N_q^m = N_m$ for $q = 1, 2, \cdots, M$) and the dispersal matrix $\mathbf{E}$ is symmetric, we can obtain two equilibria by letting the right-hand side of Eqs. (16)-(21) be zero. The female group sizes do not have to be the same. Note that, although looking complicated, the right-hand side of equations for $S_j^s(t)$ decreases with I_k^s and H_k^s, the right-hand side of equations for $I_j^s(t)$ increases with I_k^s and H_k^s. We obtain the disease-free trivial equilibrium as follows:

$$S_j^f = 1, I_j^f = 0, H_j^f = 0, \text{ for } j = 1, 2, \cdots, F, \tag{39}$$
$$S_p^m = 1, I_p^m = 0, H_p^m = 0, \text{ for } p = 1, 2, \cdots, M. \tag{40}$$

The other trivial equilibrium with disease is:

$$S_j^f = 0, I_j^f = 1, H_j^f = \frac{\alpha}{\delta}, \text{ for } j = 1, 2, \cdots, F, \tag{41}$$
$$S_p^m = 0, I_p^m = 1, H_p^m = \frac{\alpha}{\delta}, \text{ for } p = 1, 2, \cdots, M. \tag{42}$$

3. Spreading speed

The spreading speed for our system is the speed at which initially localized infection data will spread spatially, asymptotically in time. In other words, a moving reference frame traveling outwards from the initial infection at a speed faster than the spreading speed will eventually see no infection, while a moving reference frame traveling outwards from the initial infection at a speed slower than the spreading speed will eventually encounter the region of established infection. Spreading speed calculations normally require spatially homogeneous environmental conditions for the disease to spread into (but see, for example, Garlick et al. (2014)). Recall that, in sections 2.6 and 2.7, we required male groups to be of the same size. In this section, we put more restrictions and choose a special spatial arrangement of groups: we assume an equal number of female groups and male groups evenly spaced, with the home range center of a female group as the home range center of a male group and distance between the centers of neighbouring groups is set to the same, denoted by Δx. Female groups are of the same size N_f, and male groups are of the same size N_m. We choose such an arrangement as a reasonable example for which we can consider the spreading speed of the disease into a spatially homogeneous population.

We take two approaches to the spreading speed, one computational and the other theoretical. The computational approach approximates the spreading speed in a finite domain using numerical simulations where there are a finite number of groups. Then, we turn to the case of the theoretical spreading speed, which is applicable to an infinite spatial domain and with an infinite number of groups. The theoretical approach follows the classic theory of spatial systems with linearly determined spreading speeds (Lewis et al., 2016). It focuses on the rate of spread of the disease at low disease prevalence found at the leading edge of the disease invasion, and uses a linearization approach. The relationship between the traveling wave speed c and wave steepness s, referred to as a dispersion relation, is calculated for the linearized problem and then the spreading speed is given as the minimum speed for the traveling wave solution, minimized over all possible wave steepnesses (Lewis et al., 2016). Although this approach is widely used in theoretical biology (Kot et al., 1996; Lin et al., 2003; Lewis et al., 2006; Lee et al., 2008; Maidana et al., 2008; Lewis et al., 2018), our approach is informal in that, in this paper, we do not prove rigorously that minimum traveling wave speed for the linearized system yields the spreading speed for the nonlinear system. We leave this for later work. We do, however, compare the theoretical predictions to the numerical approximations over a range of model parameter values.

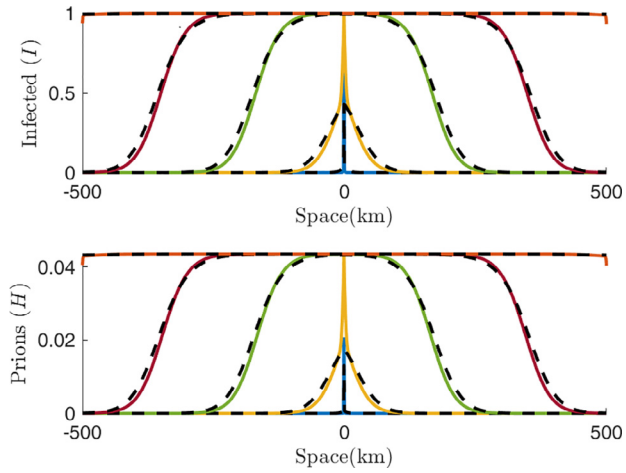

Fig. 3. The infected fraction of hosts in female and male groups (upper panel) and environmental prions shed by females and males (lower panel). Different colors of solid curves shows the status of infection at time 0.2479, 11.6804, 30.1797, 49.6260 and 75.0642 ordered from the middle to the sides, and black dashed curve near them are for male groups at the corresponding time. Parameters are set to $\beta = 0.0326\,\text{yr}^{-1}$, $\phi = 0.787\,\text{mass}^{-1}\text{yr}^{-1}$, $N_m = 2$, $N_f = 4$, $b_m = 1\,\text{km}^2\text{yr}^{-1}$, $b_f = 1.4979\,\text{km}^2\text{yr}^{-1}$, $c_2 = 0.2$, $\Delta x = 1\,\text{km}$, $\alpha = 0.111\,\text{yr}^{-1}$, $\delta = 2.55\,\text{yr}^{-1}$. Most of the parameter values are chosen based on previous studies (see Table C.1), and others are estimated.

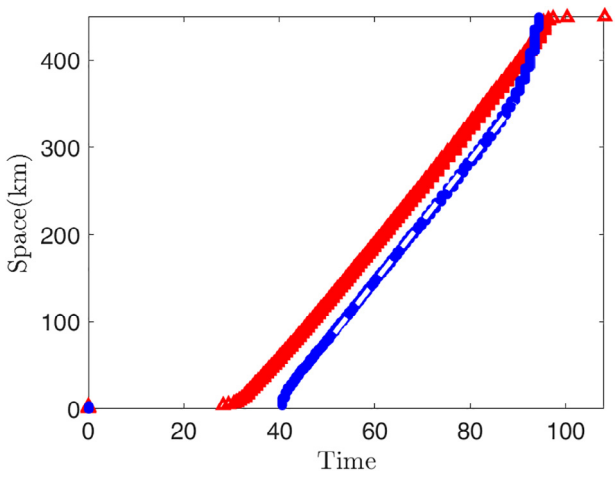

Fig. 5. The spatio-temporal spread of disease. Red triangles are for female groups, and blue stars are for male groups. For example, a red triangle placed at (x,y) means the infected fraction of the female group at location y reaches a threshold (in our case, we set the threshold to 99.99% – other thresholds can be used but the computation of speed will not change much) at time x. Points along the dashed line are used to compute the spreading speed, which is the slope of the dashed line. Here, the spreading speed is approximately 6.9635 km/yr. Parameters are set to $\beta = 0.0326\,\text{yr}^{-1}$, $\phi = 0.787\,\text{mass}^{-1}\text{yr}^{-1}$, $N_m = 2$, $N_f = 4$, $b_m = 1\,\text{km}^2\text{yr}^{-1}$, $b_f = 1.4979\,\text{km}^2\text{yr}^{-1}$, $c_2 = 0.2$, $\Delta x = 1\,\text{km}$, $\alpha = 0.111\,\text{yr}^{-1}$, $\delta = 2.55\,\text{yr}^{-1}$ (see Table C.1).

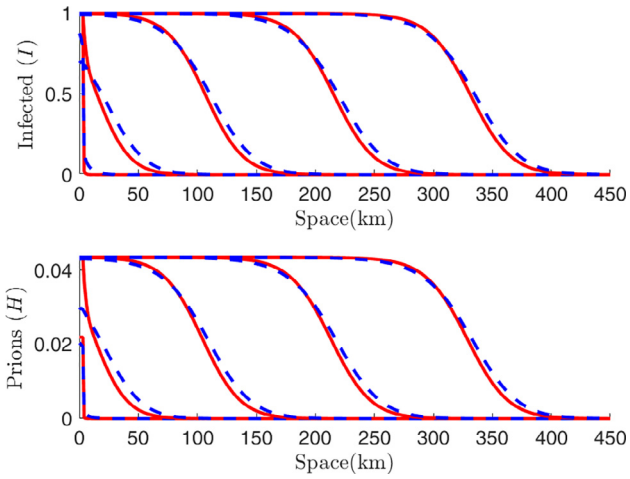

Fig. 4. The traveling wave of infected fraction of hosts in female and male groups (upper panel) and environmental prions shed by females and males (lower panel) at time 0.2759, 9.4582, 24.4005, 40.6578 and 57.3946. Red solid curves are for female groups, and blue dashed curves for male. The infection is introduced to four male groups and four female groups near the origin. Parameters are set to $\beta = 0.0326\,\text{yr}^{-1}$, $\phi = 0.787\,\text{mass}^{-1}\text{yr}^{-1}$, $N_m = 2$, $N_f = 4$, $b_m = 1\,\text{km}^2\text{yr}^{-1}$, $b_f = 1.4979\,\text{km}^2\text{yr}^{-1}$, $c_2 = 0.2$, $\Delta x = 1\,\text{km}$, $\alpha = 0.111\,\text{yr}^{-1}$, $\delta = 2.55\,\text{yr}^{-1}$ (see Table C.1).

3.1. Numerical simulations

First, we illustrate the spread of CWD that would be expected via numerical simulations on a finite domain, where the spreading speed is numerically approximated. Appendix E provides an example of the numerical simulation of spreading speed.

In these simulations the 95% radius of the home range r is used to determine the parameter b that is needed in the calculation of the home range overlap via Eqs. (2) and (10). For females we choose a 95% radius of $r_f = 2$, which gives $b_f = 1.4979$ via Eq. (4) and for males we choose a 95% radius of $r_m = 3$, which gives $b_m = 0.9986$ via Eq. (4). $b_f > b_m$ means male groups have a larger home range size (see Fig. 2). For a special case that CWD is introduced to the origin where both the female group and the male group located near the origin are infected, CWD spreads out to other places around the origin in a wave-like pattern (see Fig. 3).

To make it easier to obtain an approximation of the spreading speed numerically, we look at the case where the disease starts from one the left side of the domain (near the origin point on the left, see Fig. 4) where deer in four female groups and four male groups near the origin are all infected. We use the simulated infection levels of each group and the time of infection to compute an approximated spreading speed (Fig. 5). For each male and female group, which we track separately, we record the time at which the infection fraction of the group reaches 99.99%, relative to the locations where each group centers around. We choose 99.99% for convenience, but other thresholds will not change the outcome because the shape approaches a traveling wave as time goes on. Then, as there are both a female group and a male group for each location and we track them separately, we decided to record the time of the group that reaches the threshold later in time (in our case, it is the male group most of the time). Finally, we use the middle section of the points to fit a straight line where the least square slope of the line approximates spreading speed.

3.2. Deriving the spreading speed analytically

Because computations of the spreading speed with a large set of parameters are time demanding, we also provide the analytical approach as a means to obtain the spreading speed from traveling wave, considering the system on the infinite domain. Then, we rewrite the system as follows, using j, k as indices of females, and p, q for males:

$$\frac{d}{dt}S_j^f(t) = -S_j^f(t)\sum_{k=-\infty}^{\infty}\left(I_k^f(t)\beta_{jk}^f + H_k^f(t)\phi_{jk}^f\right)N_f - S_j^f(t)\sum_{q=-\infty}^{\infty}\left(I_q^m(t)\beta_{jq}^{fm} + H_q^m(t)\phi_{jq}^{fm}\right)N_m, \tag{43}$$

$$\frac{d}{dt}I_j^f(t) = S_j^f(t)\sum_{k=-\infty}^{\infty}\left(I_k^f(t)\beta_{jk}^f + H_k^f(t)\phi_{jk}^f\right)N_f + S_j^f(t)\sum_{q=-\infty}^{\infty}\left(I_q^m(t)\beta_{jq}^{fm} + H_q^m(t)\phi_{jq}^{fm}\right)N_m, \tag{44}$$

$$\frac{d}{dt}H_j^f(t) = \alpha I_j^f(t) - \delta H_j^f(t), \tag{45}$$

$$\frac{d}{dt}S_p^m(t) = -S_p^m(t)\sum_{k=-\infty}^{\infty}\left(I_k^f(t)\beta_{pk}^{mf} + H_k^f(t)\phi_{pk}^{mf}\right)N_f - S_p^m(t)\sum_{q=-\infty}^{\infty}\left(I_q^m(t)\beta_{pq}^m + H_q^m(t)\phi_{pq}^m\right)N_m + \sum_{q\neq p}e_{pq}S_q^m(t)N_m - S_p^m(t)N_m\sum_{q\neq p}e_{qp}, \tag{46}$$

$$\frac{d}{dt}I_p^m(t) = S_p^m(t)\sum_{k=-\infty}^{\infty}\left(I_k^f(t)\beta_{pk}^{mf} + H_k^f(t)\phi_{pk}^{mf}\right)N_f + S_p^m(t)\sum_{q=-\infty}^{\infty}\left(I_q^m(t)\beta_{pq}^m + H_q^m(t)\phi_{pq}^m\right)N_m + \sum_{q\neq p}e_{pq}I_q^m(t)N_m - I_p^m(t)N_m\sum_{q\neq p}e_{qp}, \tag{47}$$

$$\frac{d}{dt}H_p^m(t) = \alpha I_p^m(t) - \delta H_p^m(t), \tag{48}$$

$$j\in\mathbb{Z},\ p\in\mathbb{Z}, \tag{49}$$

where

$$\beta_{jq}^{fm} = \beta^{fm}\mu_{jq}^{fm}, \tag{50}$$

$$\phi_{jq}^{fm} = \phi^{fm}\mu_{jq}^{fm}, \tag{51}$$

$$\mu_{jq}^{fm} = \int_R u_j^f(\xi)u_q^m(\xi)d\xi, \tag{52}$$

$$\beta_{pk}^{mf} = \beta^{mf}\mu_{pk}^{mf}, \tag{53}$$

$$\phi_{pk}^{mf} = \phi^{mf}\mu_{pk}^{mf}, \tag{54}$$

$$\mu_{pk}^{mf} = \int_R u_p^m(\xi)u_k^f(\xi)d\xi, \tag{55}$$

$$\beta_{jk}^{s} = \beta^{s}\mu_{jk}^{s}, \tag{56}$$

$$\phi_{jk}^{s} = \phi^{s}\mu_{jk}^{s}, \tag{57}$$

$$\mu_{jk}^{s} = \int_R u_j^s(\xi)u_k^s(\xi)d\xi, \tag{58}$$

$$s = f, m. \tag{59}$$

Note that the Eqs. (43)-(48) are different from Eqs. (16)-(21). The space is extended to infinity in this model, and the group sizes of each sex are equal, N_f for females and N_m for males.

3.2.1. Pairwise host encounter rates

The pairwise host encounter rates (see Eqs. (52), (55) and (58)) are essential for transmission. To obtain these rates from the integrals, we first recall that the probability density of group j is $u_j(x) = \frac{b_j}{2}\exp(-b_j|x-x_j|)$. Then, we substitute the probability expressions of $u_j(x)$ and $u_k(x)$ into Eqs. (52), (55), and (58). We assume groups of the same sex have the same b value, so the pairwise encounter rate between two same-sex individuals from different groups j and k (Eqs. (52) and (55)) is simplified into

$$\mu_{jk}^{f/m} = \frac{b}{4}\left(1 + (|x_k - x_j|)b\right)\exp\left(-b(|x_k - x_j|)\right). \tag{60}$$

For a female and a male from different groups j and k, the encounter rate (Eq. (58)) is

$$\mu_{jk}^{fm/mf} = \frac{b_j b_k}{2\left(b_k^2 - b_j^2\right)}\left(-b_j\exp\left(-b_k(x_k - x_j)\right) + b_k\exp\left(-b_j(x_k - x_j)\right)\right). \tag{61}$$

In the special case of (61), when these two individuals have the same home range center, the encounter rate is simplified into

$$\mu_{jk}^{fm/mf} = \frac{b_j b_k}{2(b_k + b_j)}. \tag{62}$$

In Eqs. (60)–(62), parameters b, b_j, and b_k take the value of b_f for females and b_m for males. (See Appendix I for derivations of Eqs. (60)–(62).)

We can obtain the effect of changing the home range size by using Eqs. (4) and (60)–(62), e.g., if the home range radius of female groups is 3 km and group j and group k is 5 km apart, then $b_f \approx 1$, which means the pairwise between-group contact rate is $\mu_{jk}^f \approx 0.01$ and the pairwise within-group contact rate is $\mu_{jj}^f = 0.25$; if the home range radius of female groups is 2 km and group j and group k is 5 km apart, then $b_f \approx 1.5$, which means the pairwise between-group contact rate is $\mu_{jk}^f \approx 0.002$ and the pairwise within-group contact rate is $\mu_{jj}^f = 0.375$.

3.2.2. Boundary conditions and initial conditions

The natural boundary conditions for the model on the infinite domain are:

$$\lim_{j\to-\infty}S_j^f(t) = 0,\ \lim_{j\to-\infty}I_j^f(t) = 1,\ \lim_{j\to-\infty}H_j^f(t) = \frac{\alpha}{\delta}, \tag{63}$$

$$\lim_{p\to-\infty}S_p^m(t) = 0,\ \lim_{p\to-\infty}I_p^m(t) = 1,\ \lim_{p\to-\infty}H_p^m(t) = \frac{\alpha}{\delta}. \tag{64}$$

$$\lim_{j\to\infty}S_j^f(t) = 1, \lim_{j\to\infty}I_j^f(t) = 0, \lim_{j\to\infty}H_j^f(t) = 0, \tag{65}$$

$$\lim_{p\to\infty}S_p^m(t) = 1, \lim_{p\to\infty}I_p^m(t) = 0, \lim_{p\to\infty}H_p^m(t) = 0. \tag{66}$$

We do not need the initial conditions to obtain the spreading speed analytically, but, for completeness, we list them here as follows:

$$S_j^f(0) = S_{j,0}^f, I_j^f(0) = I_{j,0}^f, H_j^f(0) = H_{j,0}^f, \text{ for} j\in\mathbb{Z}, \tag{67}$$

$$S_p^m(0) = S_{p,0}^m, I_p^m(0) = I_{p,0}^m, H_p^m(0) = H_{p,0}^m, \text{ for} p\in\mathbb{Z}. \tag{68}$$

3.2.3. Linearization

We linearize the system around the disease-free equilibrium by substituting the following into the system:

$$S = 1 - \tilde{S}, I = \tilde{I}, H = \tilde{H}, \tag{69}$$

and keep only linear terms. Note that there is a negative sign before $\tilde{S}$, where $\tilde{S}$ represents the lost fraction of the susceptible hosts due to initial infection. For illustration only, a simplified ODE for $\tilde{S}$ looks like

$$-\frac{d}{dt}\tilde{S} = -\left(1-\tilde{S}\right)\left[\sum_k\left(\tilde{I}\beta + \tilde{H}\phi\right)N + \sum_q\left(\tilde{I}\beta + \tilde{H}\phi\right)N\right] \tag{70}$$

$$\approx -\left[\sum_k\left(\tilde{I}\beta + \tilde{H}\phi\right)N + \sum_q\left(\tilde{I}\beta + \tilde{H}\phi\right)N\right]. \tag{71}$$

For simplicity, we use S to denote $\tilde{S}$ in the following (as well as droping the tildes on I and H). As the original ODE for pairs of S and I sum to a constant, we only keep the ODE of Iin the following. So, we obtain

$$\frac{d}{dt}I_j^f(t) = \sum_{k=-\infty}^{\infty}\left(I_k^f(t)\beta_{jk}^f + H_k^f(t)\phi_{jk}^f\right)N_f + \sum_{q=-\infty}^{\infty}\left(I_q^m(t)\beta_{jq}^{fm} + H_q^m(t)\phi_{jq}^{fm}\right)N_m, \tag{72}$$

$$\frac{d}{dt}H_j^f(t) = \alpha I_j^f(t) - \delta H_j^f(t), \tag{73}$$

$$\frac{d}{dt}I_p^m(t) = \sum_{k=-\infty}^{\infty}\left(I_k^f(t)\beta_{pk}^{mf} + H_k^f(t)\phi_{pk}^{mf}\right)N_f + \sum_{q=-\infty}^{\infty}\left(I_q^m(t)\beta_{pq}^{m} + H_q^m(t)\phi_{pq}^{m}\right)N_m + \sum_{q\neq p}e_{pq}I_q^m(t)N_m - I_p^m(t)N_m\sum_{q\neq p}e_{qp}, \tag{74}$$

$$\frac{d}{dt}H_p^m(t) = \alpha I_p^m(t) - \delta H_p^m(t). \tag{75}$$

3.2.4. Spatially homogeneous infection dynamics

For the disease to spread spatially when introduced locally we require that CWD will grow when introduced into an uninfected population in a spatially homogeneous manner. The condition for infection growth is equivalent to the condition under which the trivial equilibrium $[0,0,0,0]^T$ for the spatially homogeneous system is unstable. That means the Jacobian matrix evaluated at the trivial equilibrium should have at least one eigenvalue with a nonnegative real part. Now we revisit our model in Eqs. (72) and (75) and assume homogeneous infection and prion levels, so that we obtain

$$\frac{d}{dt}I^f(t) = \left(I^f(t)\sum_{k=-\infty}^{\infty}\beta_{jk}^f + H^f(t)\sum_{k=-\infty}^{\infty}\phi_{jk}^f\right)N_f + \left(I^m(t)\sum_{q=-\infty}^{\infty}\beta_{jq}^{fm} + H^m(t)\sum_{q=-\infty}^{\infty}\phi_{jq}^{fm}\right)N_m, \tag{76}$$

$$\frac{d}{dt}H^f(t) = \alpha I^f(t) - \delta H^f(t), \tag{77}$$

$$\frac{d}{dt}I^m(t) = \left(I^f(t)\sum_{k=-\infty}^{\infty}\beta_{pk}^{mf} + H^f(t)\sum_{k=-\infty}^{\infty}\phi_{pk}^{mf}\right)N_f + \left(I^m(t)\sum_{q=-\infty}^{\infty}\beta_{pq}^{m} + H^m(t)\sum_{q=-\infty}^{\infty}\phi_{pq}^{m}\right)N_m + I^m(t)N_m\sum_{q\neq p}e_{pq} - I^m(t)N_m\sum_{q\neq p}e_{qp}, \tag{78}$$

$$\frac{d}{dt}H^m(t) = \alpha I^m(t) - \delta H^m(t). \tag{79}$$

As we assume symmetric dispersal, i.e., $e_{qp} = e_{pq}$, the dispersal terms cancel in the $I^m(t)$ equation, leading to the following system:

$$\frac{d}{dt}I^f(t) = \left(I^f(t)\sum_{k=-\infty}^{\infty}\beta_{jk}^f + H^f(t)\sum_{k=-\infty}^{\infty}\phi_{jk}^f\right)N_f + \left(I^m(t)\sum_{q=-\infty}^{\infty}\beta_{jq}^{fm} + H^m(t)\sum_{q=-\infty}^{\infty}\phi_{jq}^{fm}\right)N_m, \tag{80}$$

$$\frac{d}{dt}H^f(t) = \alpha I^f(t) - \delta H^f(t), \tag{81}$$

$$\frac{d}{dt}I^m(t) = \left(I^f(t)\sum_{k=-\infty}^{\infty}\beta_{pk}^{mf} + H^f(t)\sum_{k=-\infty}^{\infty}\phi_{pk}^{mf}\right)N_f + \left(I^m(t)\sum_{q=-\infty}^{\infty}\beta_{pq}^{m} + H^m(t)\sum_{q=-\infty}^{\infty}\phi_{pq}^{m}\right)N_m, \tag{82}$$

$$\frac{d}{dt}H^m(t) = \alpha I^m(t) - \delta H^m(t). \tag{83}$$

We rewrite the system into the matrix form in the following:

$$\frac{d}{dt}\begin{bmatrix} I^f(t) \\ H^f(t) \\ I^m(t) \\ H^m(t) \end{bmatrix} = W\begin{bmatrix} I^f(t) \\ H^f(t) \\ I^m(t) \\ H^m(t) \end{bmatrix}, \tag{84}$$

where $W = (w_{jk})$ is

$$\begin{bmatrix} N_f\sum_{k=-\infty}^{\infty}\beta_{jk}^f & N_f\sum_{k=-\infty}^{\infty}\phi_{jk}^f & N_m\sum_{q=-\infty}^{\infty}\beta_{jq}^{fm} & N_m\sum_{q=-\infty}^{\infty}\phi_{jq}^{fm} \\ \alpha & -\delta & 0 & 0 \\ N_f\sum_{k=-\infty}^{\infty}\beta_{pk}^{mf} & N_f\sum_{k=-\infty}^{\infty}\phi_{pk}^{mf} & N_m\sum_{q=-\infty}^{\infty}\beta_{pq}^{m} & N_m\sum_{q=-\infty}^{\infty}\phi_{pq}^{m} \\ 0 & 0 & \alpha & -\delta \end{bmatrix}. \tag{85}$$

Note that $w_{jk} \geqslant 0$ for $j \neq k$, i.e., all the off-diagonal entries of W are nonnegative, so W is a Metzler matrix (see, e.g., Ngoc, 2006). Using the properties of the matrix exponential and Gronwall's Inequality (Gronwall, 1919), we show that the trivial equilibrium is unstable in Appendix B.

3.2.5. Traveling wave ansatz

We consider traveling wave solutions to the linearized system (72)-(75). Because the system is linear we write the traveling wave solutions in the following form (exponentially decaying traveling wave ansatz):

$$I_j^f = K_1\exp(-s(j\Delta x - ct)), \tag{86}$$

$$H_j^f = K_2\exp(-s(j\Delta x - ct)), \tag{87}$$

$$I_p^m = K_3\exp(-s(p\Delta x - ct)), \tag{88}$$

$$H_p^m = K_4\exp(-s(p\Delta x - ct)), \tag{89}$$

where the parameters K_i $(i = 1, 2, 3, 4)$ are constants, s determines the shape of the traveling wave solutions and c determines the speed. Our goal is to derive a dispersion relation between c and s for this traveling wave problem $(c = c(s))$ and then to equate the spreading speed with the minimum possible traveling wave speed $(\min_s c(s))$.

We first substitute the above form of solutions into Eqs. (72)-(75), and obtain equations for constants K_i:

$$csK_1 = N_f\left(\beta^f K_1 + \phi^f K_2\right)L_j^f(s) + N_m\left(\beta^{fm}K_3 + \phi^{fm}K_4\right)L_j^{fm}(s), \tag{90}$$

$$csK_2 = \alpha K_1 - \delta K_2, \tag{91}$$

$$csK_3 = N_f\left(\beta^{mf}K_1 + \phi^{mf}K_2\right)L_p^{mf}(s) + N_m(\beta^m K_3 + \phi^m K_4)L_p^m(s) + N_m K_3 J_p^m(s), \tag{92}$$

$$csK_4 = \alpha K_3 - \delta K_4, \tag{93}$$

where

$$L_j^f(s) = \exp(sj\Delta x)\sum_{k=-\infty}^{\infty}\mu_{jk}^f\exp(-sk\Delta x), \tag{94}$$

$$L_j^{fm}(s) = \exp(sj\Delta x)\sum_{q=-\infty}^{\infty}\mu_{jq}^{fm}\exp(-sq\Delta x), \tag{95}$$

$$L_p^{mf}(s) = \exp(sp\Delta x)\sum_{k=-\infty}^{\infty}\mu_{pk}^{mf}\exp(-sk\Delta x), \tag{96}$$

$$L_p^m(s) = \exp(sp\Delta x)\sum_{q=-\infty}^{\infty}\mu_{pq}^m\exp(-sq\Delta x), \tag{97}$$

$$J_p^m(s) = \exp(sp\Delta x)\sum_{q\neq p}e_{pq}\exp(-sq\Delta x) - \sum_{q\neq p}e_{qp}. \tag{98}$$

Eqs. (94)-(98) can be simplified using the formula for a geometric series (see Appendix D). Thus, we obtain a system of the constants K_i

$$A\begin{bmatrix}K_1\\K_2\\K_3\\K_4\end{bmatrix}=0, \tag{99}$$

where A is

$$\begin{bmatrix}N_f\beta^f L_j^f(s)-cs & N_f\phi^f L_j^f(s) & N_m\beta^{fm}L_j^{fm}(s) & N_m\phi^{fm}L_j^{fm}(s)\\ \alpha & -\delta-cs & 0 & 0\\ N_f\beta^{mf}L_p^{mf}(s) & N_f\phi^{mf}L_p^{mf}(s) & a_{33} & N_m\phi^m L_p^m(s)\\ 0 & 0 & \alpha & -\delta-cs\end{bmatrix}, \tag{100}$$

with $a_{33}=N_m\beta^m L_p^m(s)+N_m J_p^m(s)-cs$.

In order to make sure the traveling wave solutions are nontrivial, a non-zero solution of K_i needs to exist, which means $\det(A)=0$ must hold. Then, the implicit relation between s and c is obtained from $\det(A)=0$. Once we obtain an expression of c in terms of s, the minimum value of c is the spreading speed.

3.2.6. Calculating the spreading speed mathematically

We revisit the matrix in Eq. (100), and rewrite it as

$$A=\widehat{A}-cs\begin{bmatrix}1&0&0&0\\0&1&0&0\\0&0&1&0\\0&0&0&1\end{bmatrix}, \tag{101}$$

where $\widehat{A}$ is the following matrix:

$$\begin{bmatrix}N_f\beta^f L^f(s) & N_f\phi^f L^f(s) & N_m\beta^{fm}L^{fm}(s) & N_m\phi^{fm}L^{fm}(s)\\ \alpha & -\delta & 0 & 0\\ N_f\beta^{mf}L^{mf}(s) & N_f\phi^{mf}L^{mf}(s) & N_m\beta^m L^m(s)+N_m J^m(s) & N_m\phi^m L^m(s)\\ 0 & 0 & \alpha & -\delta\end{bmatrix} \tag{102}$$

Then the problem of $\det(A(c,s))=0$ can be turned into

$$\det\left(\widehat{A}(s)-csI\right)=0, \tag{103}$$

where cs is the eigenvalue of the matrix $\widehat{A}$. In the meantime, Eq. (99) is equivalent to

$$\left(\widehat{A}(s)-csI\right)\vec{K}=0, \tag{104}$$

or,

$$\widehat{A}(s)\vec{K}=cs\vec{K}, \tag{105}$$

so that cs is the eigenvalue of $\widehat{A}$, and the vector $\vec{K}=[K_1,K_2,K_3,K_4]^T$ is the associated eigenvector.

Theorem 1. *The matrix* $\widehat{A}$ in Eq. (102) *has the following properties:*

(i) *there exists a positive real eigenvalue* λ *that is associated with a positive eigenvector* $\vec{v}$*;*

(ii) *this eigenvalue* λ *is simple and is the spectral abscissa of* $\widehat{A}$*;*

(iii) *there are no other positive eigenvectors other than the vector* $\vec{v}$ *and its positive multiples.*

Proof. We rewrite (102) as

$$\begin{bmatrix}a_{11}&a_{12}&a_{13}&a_{14}\\ \alpha&-\delta&0&0\\ a_{31}&a_{32}&a_{33}&a_{34}\\ 0&0&\alpha&-\delta\end{bmatrix}, \tag{106}$$

where

$$a_{11}=N_f\beta^f L^f(s), \tag{107}$$
$$a_{12}=N_f\phi^f L^f(s), \tag{108}$$
$$a_{13}=N_m\beta^{fm}L^{fm}(s), \tag{109}$$
$$a_{14}=N_m\phi^{fm}L^{fm}(s), \tag{110}$$
$$a_{31}=N_f\beta^{mf}L^{mf}(s), \tag{111}$$
$$a_{32}=N_f\phi^{mf}L^{mf}(s), \tag{112}$$
$$a_{33}=N_m\beta^m L^m(s)+N_m J^m(s), \tag{113}$$
$$a_{34}=N_m\phi^m L^m(s). \tag{114}$$

Because all the a_{ij} values are positive and $\alpha,\delta>0$, we can use a similar method used at the end of Section 3.2.4 (see Appendix B) to prove that the spectral abscissa $\gamma\left(\widehat{A}\right)$ is positive. Note that all the off-diagonal entries of $\widehat{A}$ are nonnegative, so $\widehat{A}$ is a Metzler matrix (see, e.g., Ngoc, 2006). We use the properties of Metzler matrix to justify the rest of the proposition.

We first translate $\widehat{A}$ to a nonnegative matrix by adding a positive multiple of identity δI. A simple calculation shows $\left(\widehat{A}+\delta I\right)^2>0$, and so $\widehat{A}+\delta I$ is a primitive matrix (Meyer et al., 2000, (8.3.16)). By definition, a primitive matrix is nonnegative and irreducible (Horn et al., 2012, Definition 8.5.0). By the Perron Frobenius theorem for irreducible and nonnegative matrices (Horn et al., 2012, Theorem 8.4.4), there exists a simple positive eigenvalue for $\left(\widehat{A}+\delta I\right)$ that is equal to the spectral radius $\rho\left(\widehat{A}+\delta I\right)$, and the associated left eigenvector and right eigenvector are both positive. Because $\widehat{A}+\delta I$ is primitive, all other eigenvalues have smaller modulus (Horn et al., 2012, Lemma 8.4.3). Therefore, we have

$$\left(\widehat{A}+\delta I\right)\vec{v}=\rho\left(\widehat{A}+\delta I\right)\vec{v}, \tag{115}$$

that is,

$$\widehat{A}\vec{v}=\left(\rho\left(\widehat{A}+\delta I\right)-\delta\right)\vec{v}. \tag{116}$$

Hence, the Metzler matrix $\widehat{A}$ has a simple eigenvalue $\gamma\left(\widehat{A}\right)=\rho\left(\widehat{A}+\delta I\right)-\delta$ (Hinrichsen et al., 1998). Because we have subtracted delta from the spectral radius of $\widehat{A}+\delta I$, $\gamma\left(\widehat{A}\right)$ may not be the spectral radius of $\widehat{A}$. However, it yields the spectral abscissa of $\widehat{A}$, $\gamma\left(\widehat{A}\right)$. The associated eigenvector of $\widehat{A}$ is the same as the eigenvector of $\widehat{A}+\delta I$, so the entries of the eigenvector associated with $\gamma\left(\widehat{A}\right)$ are positive. □

By now we have shown that the spectral abscissa of the matrix $\widehat{A}(s)$ exists and is a positive and simple eigenvalue, and its corresponding eigenvector is positive. Hence, c can be expressed in terms of s following Eq. (105):

$$c(s)=\frac{1}{s}\gamma\left[\widehat{A}(s)\right], \tag{117}$$

The spreading speed is expressed as the minimum value that $c(s)$ can attain:

$$\min_{s\in\Omega}\left(\frac{1}{s}\gamma\left[\widehat{A}(s)\right]\right), \tag{118}$$

where $\Omega = (0, \min\{b_m, b_f, c_2\})$. Although we can simplify the series in $\widehat{A}$ (see Appendix D), it is hard to obtain the analytical expression of the spreading speed explicitly. Therefore, we minimize Eq. (118) numerically to calculate the spreading speed.

3.2.7. Local sensitivity analysis

Many of the parameters have a positive effect on the spreading speed, but their relative importance is not clear. In sensitivity analysis (Saltelli et al., 2004), we use σ to denote the sensitivity of the spreading speed (y) in response to the perturbed parameters. Here, we look at the local sensitivity, for example, we perturb the prion shedding rate α, around a nominal value, $\alpha_{nominal} = 0.111$, by 1%; then we evaluate the spreading speed at the nominal value and the new value of α with all the other parameters kept the same; then we compare the relative change of spreading speed to the relative change of α by taking a ratio:

$$\sigma = \frac{(y_{new} - y_{nominal})/y_{nominal}}{(\alpha_{new} - \alpha_{nominal})/\alpha_{nominal}} \tag{119}$$

$$= \frac{(y(1.01 * \alpha_{nominal}) - y(\alpha_{nominal}))/y(\alpha_{nominal})}{(1.01 * \alpha_{nominal} - \alpha_{nominal})/\alpha_{nominal}}. \tag{120}$$

Note: $\sigma = 1$ means the spreading speed increases by 1% when α increases by 1% from the nominal value; $\sigma = 2$ means the spreading speed increases by 2% when α increases by 1% from the nominal value. Larger absolute value of σ means the output is more sensitive to the change of parameter, i.e., the parameter has a larger impact on the output, which is the spreading speed in our case.

3.2.8. Multiple parameters: edge effects on deer home range size and deer density

Recall that edge density is a metric of landscape heterogeneity (see Appendix J). Here we examine the effect of edge density on the spreading speed when the home range size and deer density are affected by edge density at the same time, as an example of how our model could be used to assess the effect of landscape heterogeneity in 1D space. Once we extend the model to 2-dimensional space (in preparation), this application will be more meaningful. Empirical studies found that the natural log of home range size is negatively correlated with edge density (Walter et al., 2018), and deer density is positively correlated with edge density (Plante et al., 2004). We choose parameters to match the range of home range size (in 2D) and deer density in (Merrill et al., 2011). The 95% home range in 1D space is assumed to be equal to the diameter of the home range in 2D, using the following relationships:

$$[\text{home range size in 2D}] = \exp(3 - 0.01 * [\text{edge density}]), \tag{121}$$

$$[\text{home range size in 1D}] = 2\left(\frac{[\text{home range size in 2D}]}{\pi}\right)^{\frac{1}{2}}, \tag{122}$$

We assume a linear relationship between deer density and the edge density:

$$\text{density} = 5[\text{edge density}] + 1 \tag{123}$$

Group size is shown to change with deer density, so we use the result by Habib et al. (2011):

$$\ln(\text{group size}) = 1.206 + 0.250\ln(\text{density}). \tag{124}$$

4. Results

4.1. Numerical vs. analytical-based spreading speed

Under the specific conditions of deer distributions, grouping assumptions, and the default parameters, the numerical simulation result of the spreading speed of 6.9635 km/year is close to the analytical result of 7.3201 km/year (Fig. 6). Further comparisons between the theoretical and numerical spreading speeds are given in Fig. 6. Because of the limited span of space and time we used in the simulations and the spatial edge effect, the numerical simulations consistently underestimated the spreading speed, which is asymptotic in time and assumes infinite space.

4.2. Effects of a single parameters on the spreading speed

We categorize the parameters of interest to us into two sets for easier reference. The first set of parameters includesthe direct transmission rate, the environmental transmission rate, the prion shedding rate, and the degrading rate of prions, which are directly relevant to CWD. We refer to them as parameters relevant to the disease in the following. The second set includes deer density, group sizes, home range size, dispersal distance of males, and the male-to-female sex ratio. Because those parameters exist for a disease-free population, we refer to them as the set of parameters relevant to the population in the following.

We first assess the effect for the set of parameters relevant to the disease. As expected, we found that β, ϕ, and α have a positive effect on the spreading speed, whereas an increase in the rate of prion degradation in the environment has a negative effect (Fig. 6). Among this set of parameters, the spreading speed is most sensitive to the direct transmission rate, whereas increasing the direct transmission rate from 0.0326 yr^{-1} by 1% will increase the spreading speed by 0.2842% (Table 2). Environmental transmission rate, prion shedding rate, and prion degrading rate have comparable although smaller sensitivities (0.2457%, 0.2457%, and −0.2012%, see Table 2).

As for the set of parameters relevant to population, we found that increasing any of them had a positive influence on the spreading speed (Fig. 7). Among all the parameters, group size (which affects deer density) and mean dispersal distance of males had the largest impact on spreading speed (see Table 2) when all other parameters were held constant at the nominal value. Increasing the group size from $N_f = 4$ and $N_m = 2$ by 1% (i.e., deer density increases by 1%) speeds up the spreading speed of CWD by 0.956%, whereas increasing the number of groups (group density) by 1% (i.e., deer density increases by 1%) speeds up the spread by 0.3598% (Table 2). Increasing the mean dispersal distance of males from 5 km by 1% speed up the spread by 0.9809% (Table 2). Perturbing the sex ratio by 1% around 0.5, 0.2 and 0.1 leads to similar changes in the spreading speed (0.3982%, 0.4220%, and 0.3869% respectively, see Table 2). Influences of home range size on spreading speed were greater when home ranges were large. For example, when the female home range radius is fixed, perturbing the male home range radius by 1% around 3 km barely changes the speed (−0.000092%), but perturbing the male home range radius around 20 kmchanges the speed up to 0.3656%. Appendix F provides a brief note for the inputs and procedure of the mathematical calculation of spreading speed.

4.3. Effect of edge density

Here we examine the effect of edge density on the spreading speed when the home range size and deer density are affected by edge density at the same time. Increasing edge density has a pos-

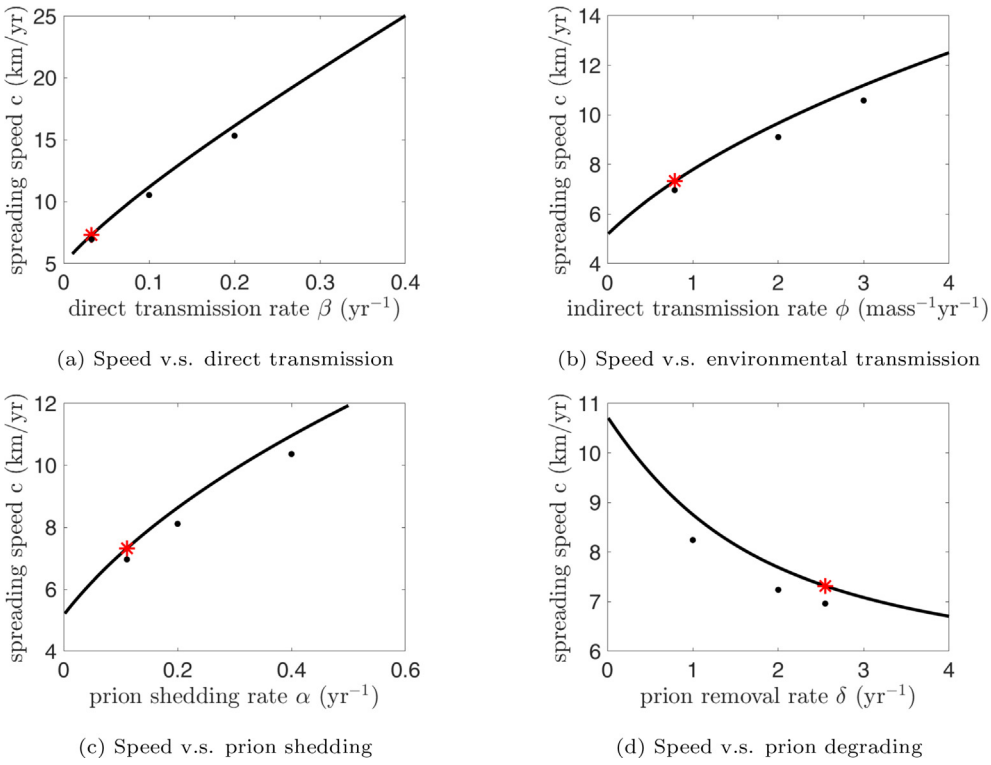

(a) Speed v.s. direct transmission

(b) Speed v.s. environmental transmission

(c) Speed v.s. prion shedding

(d) Speed v.s. prion degrading

Fig. 6. Transmission parameters β, ϕ, and α have a positive effect on the spreading speed, whereas δ has a negative effect. The numerical simulations (dots, see Section 3.1 for the method of simulation) always underestimate the analytical spreading speed (solid lines). If not specified, the parameters are set to the default: $\beta = 0.0326\,\text{yr}^{-1}, \phi = 0.787\,\text{mass}^{-1}\text{yr}^{-1}, N_m = 2, N_f = 4, b_m = 1\,\text{km}^2\text{yr}^{-1}, b_f = 1.4979\,\text{km}^2\text{yr}^{-1}, c_2 = 0.2, \Delta x = 1\,\text{km}, \alpha = 0.111\,\text{yr}^{-1}, \delta = 2.55\,\text{yr}^{-1}$. Most of the parameter values are chosen based on previous studies (see Table C.1), and others are estimated. In each panel, the star (*) shows the analytical spreading speed (7.3201 km per year) calculated using the set of given parameters; the dot below the star is the corresponding numerical simulation of 6.9635 km/year.

itive effect on the spreading speed (see Fig. 8). In addition, the slope of the curve in Fig. 8 increases as edge density increases. For instance, we look at two special cases when the forest edge density is 50 m/ha and 200 m/ha. By examining the effect of changing edge density from 200 m/ha to 190 m/ha, we found that the spreading speed is reduced by 0.0772 km/year; when changing edge density from 50 m/ha to 40 m/ha, we saw only a reduction of the spreading speed by 0.0234 km/year.

Table 2
Sensitivity of spreading speed to 1% local perturbation of parameters.

parameters	unit	value	sensitivity
direct transmission rate (β)	yr^{-1}	0.0326	0.2842
environmental transmission rate (ϕ)	mass^{-1}yr^{-1}	0.787	0.2457
shedding rate (α)	yr^{-1}	0.111	0.2457
degrading rate (δ)	yr^{-1}	2.55	−0.2012
group density per 100 km ($100/\Delta x$)	per 100 km	100	0.3598
group size multiplier*	(dimensionless)	1	0.9560
male home range radius+	km	3	-9.2e-5
		20	0.3656
mean dispersal distance of males	km	5	0.9809
male-to-female sex ratio (N_m/N_f)	(dimensionless)	0.5	0.3982
		0.2	0.4220
		0.1	0.3869

See Table C.1 for the source of parameter values for our numerical simulations.
* The group multiplier is used to get the group size for fixed sex ratio with the same number of groups for males and females. The deer density changes proportionally with it.
+ Female home range radius is fixed to 2 km. We use the radius here in 1D to mean the distance from the home range center to the edge of 95% home range. See Eq. (4).

5. Discussion

To our knowledge, the framework we presented here is the first one to incorporate deer home ranges, the group size, and the dispersal of males explicitly into the mechanistic model studying the spreading speed of the chronic wasting disease. This framework provides a base for integrating empirical studies of home ranges, the group size, and male dispersal into the analytical models. Both direct and environmental transmissions are included.

Mathematically, we undertook an informal derivation of the spreading speed for the CWD disease on this spatially discrete coupled system of ordinary differential equations. In our derivation, we made the assumption that the spreading speed was linearly determined and equivalent to the minimum possible traveling wave speed. These assumptions are consistent with the literature on simpler models for spatially discrete epidemics (Zhang et al., 2007) and also for the spatial spread in continuous space for cooperative disease dynamics, such as ours has (Lewis et al., 2006). However, it remains to rigorously prove that the assumptions are justified, and we leave this for future work.

Our numerical simulations of the spreading speed are intuitive, and we found that the analytical results show a good match with the simulations. The spreading speed from the numerical simulations was shown to be always slightly smaller than that of analytical results, because we assumed finite space and time in the simulations. The spreading speed we obtained analytically is less time-consuming and appears to provide a proper upper bound for more complicated cases when we include the demographic processes.

Given the parameterization of our model, our local sensitivity analysis (see Table 2) shows that the direct and environmental transmission rates have a positive effect on the spreading speed,

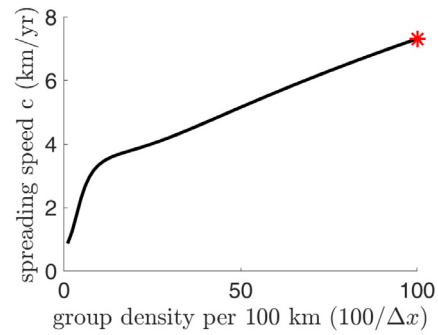

(a) Speed v.s. group density

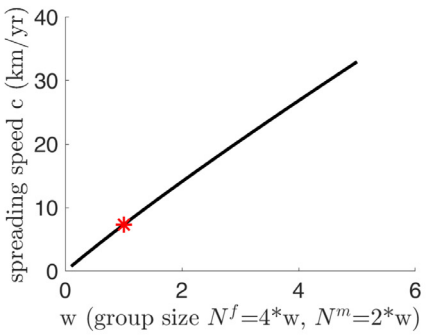

(b) Speed v.s. group size

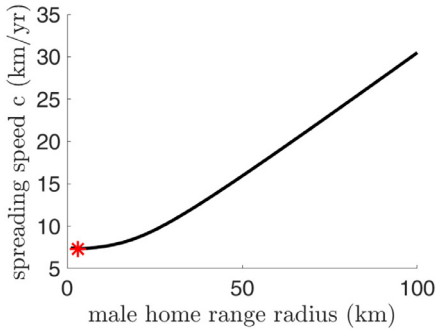

(c) Speed v.s. home range size of males (with fixed female home range radius 2km)

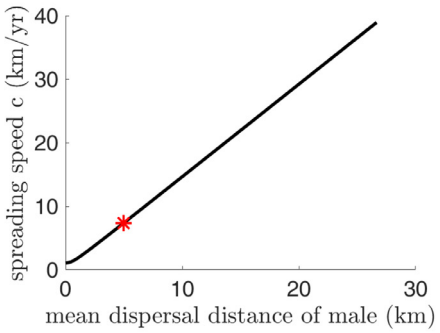

(d) Speed v.s. male dispersal

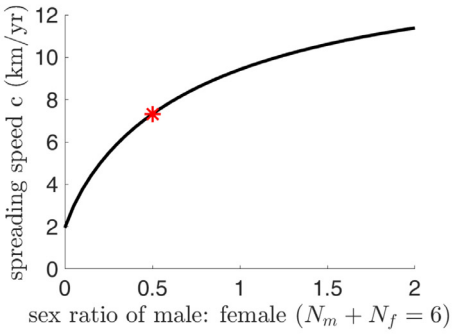

(e) Speed v.s. male-to-female sex ratio

Fig. 7. Graphs for population characteristics. Parameters are set to default values $\beta = 0.0326\,\text{yr}^{-1}$, $\phi = 0.787\,\text{mass}^{-1}\text{yr}^{-1}$, $N_m = 2$, $N_f = 4$, $b_m = 1\,\text{km}^2\text{yr}^{-1}$, $b_f = 1.4979\,\text{km}^2\text{yr}^{-1}$, $c_2 = 0.2$, $\Delta x = 1\,\text{km}$, $\alpha = 0.111\,\text{yr}^{-1}$, $\delta = 2.55\,\text{yr}^{-1}$ whenever not specified (see Table C.1).

and the direct exposure and transmission have a greater influence on the spreading speed than from the environment. The impact of direct transmission on spreading speed is 16% more. However, considering the sensitivity of the spreading speed to changes of the prion shedding rate and the prion degrading rate (0.2457 and −0.2012, which is similar to the sensitivity to the direct and environmental transmission rates), the effect of environmental transmission should not be ignored, especially for CWD-infected areas that have been exposed to prions for decades. Previous experiments of CWD bioassay inocula indicated that CWD infection could occur through blood IV, saliva, environmental exposure of preclinical and clinical CWD positive hosts (Mathiason et al., 2009). Our result supports previous studies that emphasize the need to obtain better estimates of the environmental transmission rate and prion shedding/degrading rate, to make a proper prediction of future prevalence and make management suggestions.

Few models have considered male dispersal in a spatial context due to a lack of data or technical difficulties in assessing the effect of dispersal over a large spatial and temporal scale. Our results indicate the dispersal distance of males might have a greater relative influence on the spreading speed than deer density (either by increasing group size or group density). Previous studies found that juveniles and particularly juvenile males are most likely to disperse (DeYoung, 2011): when no fawns were collared, only 4.4% of collared mule deer in southeast Alberta (n = 135) dispersed (Merrill et al., 2011), whereas 60% of male and 39% of female white-tailed deer fawns were observed to disperse in a similar agro-forested environment (Nixon et al., 2007). Although long-distance dispersals of adult male deer are rarely studied, they can be imperative in the spread of infectious disease (Moll et al., 2021), such as CWD. Indeed, because the male infection rate is high and male home ranges are usually larger than females, and we

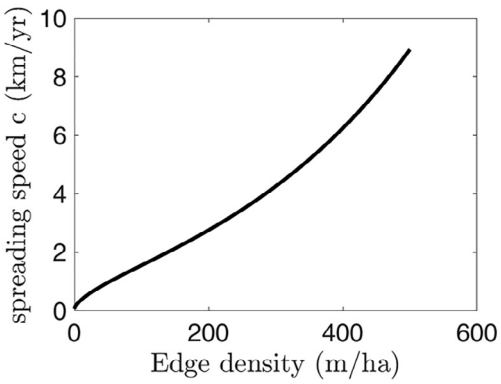

Fig. 8. Effect of edge density on the spreading speed by affecting the home range size and deer density directly. We separate the group size obtained from the Eq. (124) into female group size and male group size using a fixed sex ratio (m:f = 1:2). Then the 2D home range size is converted to 1D by taking the diameter of a circular home range. Δx, the distance between neighbouring groups are calculated using deer density and group size. Parameters are set to $\beta = 0.0326\,\mathrm{yr}^{-1}$, $\phi = 0.787\,\mathrm{mass}^{-1}\mathrm{yr}^{-1}, N_m:\ N_f = 1:2,\ c_2 = 0.2,\ \alpha = 0.111\,\mathrm{yr}^{-1},\ \delta = 2.55\,\mathrm{yr}^{-1}$ (see Table C.1).

found that home range size could have a significant impact on the spreading speed, males may contribute to the disease distribution by spreading the disease as they travel long distances. Juvenile male dispersal distance is negatively affected by forest cover (Long et al., 2005). A study in southern Saskatchewan reported juvenile mule deer dispersed 6.5 km to 195.5 km (n = 10), with an average dispersal distance of 36.9 km (see Skelton, 2010, Table 2.2). Using that dispersal distance, a buck: fawn ratio of 1:1, a sex ratio of 1:1 for fawns, and a dispersal rate of 0.55 (see Skelton, 2010, Section 2.4.1.1), we estimate the dispersal distance to be 6.8 km, so the value we use, 5 km, is comparable. Although not considered in our framework, we expect the effect of female dispersal to vary depending on the dispersal rate and distance and the size of female social groups, and the female dispersal may increase the spreading speed of CWD. Our study supports the previous genetic study, which raised the concern on the effect of deer movement on disease spread (Walter et al., 2011), especially long-distance dispersal.

Future work is in progress to include age structure. A study on the patterns of CWD infection indicates that old males ($>$ 4.5 years old) are 1.4–2 times more likely to be infected than younger males ($<$ 1.5 years old) (Samuel and Storm, 2016). Including the age structure enables us to compare the spread in different age classes, and make recommendations for age-specific harvesting strategies to manage CWD spread.

Because deer are reported to respond to forest edge density, we considered two aspects of such effect, that is, on home range size and deer density. Intuitively, a higher edge density might have a positive or a negative effect on the spread of CWD. Indeed, if higher edge density leads to a more scattered deer distribution, then there will be less overlap of deer land use, leading to less contact between groups. However, smaller home range sizes might lead to a larger probability of within-group contact (Eq. (4) implies smaller home ranges leads to a greater value of b, and setting $x_k = x_j$ in Eq. (60) gives us the encounter rate is proportional to b). On the other hand, larger deer density increases the group size and increases both within-group contact and between-group contact. However, our computational simulation (Fig. 8) shows that increasing edge density leads to a faster spread of CWD. This aligns with a previous study showing a positive correlation between forest edge density and infection rate (Storm et al., 2013).

For our choice of parameters, our simulation suggests that reducing the edge density might serve as a management strategy to slow down the spreading speed of CWD. The slope of the curve in Fig. 8 increases as edge density increases, implying that the outcome of reducing the edge density in areas with different levels of edge density may be different. The difference resulted from the effect of changing the edge density on the contact frequency among the hosts. Both the within- and between-group contact frequencies declined, as well as the within- and between-sex contact frequencies. However, starting at the edge density of 200 m/ha and reducing it by 10 m/ha, the resulting reduction of total contacts in the population is more considerable than starting at the edge density of 50 m/ha. Our method involves measuring contact rate using the encounter rates and group sizes, and this is in line with the approach in (Schauber et al., 2007) that uses the volume of intersections of home ranges to understand CWD transmission.

Despiteits importance on various aspects of deer demographics and movement, the impact of landscape heterogeneity in CWD spread is not fully understood. Our framework makes it possible to investigate this effect. Studies have shown that landscape heterogeneity influences the deer home range and other forms of spatial movement in differing scales (Kie et al., 2002; Walter et al., 2018), as well as deer density and composition. For example, in addition to affecting deer density and home range size, Skuldt et al. (2008) reported that higher edge density in the natal home range of yearling males is correlated with a higher probability of dispersal. We have includeda spatial structure in our disease-modeling framework by including home ranges, which allows us to investigate the encounter rate resulting from the spatial structure of home ranges of hosts, as a step towards a better understanding of transmission (Martinez-Garcia et al., 2020). Movement patterns of deer in 2D vary in different biological seasons, leading to critical changes in the interactions between hosts, and therefore transmission. Our mechanistic framework allows us to extend its application to 2-D in an ongoing study and use the empirical resource selection functions for home ranges, as well as including more realistic seasonal grouping patterns, especially the mixed-sex groups in winter, and demographic dynamics (i.e., age structure, birth, and deaths). Adding deer demography allows us to study the diluting effect of newborns, and the compensatory mortality (Bartmann et al., 1992) or dispersal of the population in response to disease-induced mortality. We expect that the overall result for the relative importance of factors on disease transmission might be similar in our 2D model, but the newly added factors (e.g., growth, mortality, and seasonality) may affect the outcome. For example, an increased harvest might reduce local transmission in a short time but might encourage more dispersals and lead to unfavorable long-term outcomes. This level of spatial details also allows us to apply the models at larger scales and inform the management through spatially selective harvesting.

Declaration of Competing Interest

The authors declare that they have no known competing financial interests or personal relationships that could have appeared to influence the work reported in this paper.

Acknowledgments

The authors gratefully acknowledge funding from the Wildlife Management Institute, Boone and Crockett Club, Rocky Mountain Elk Foundation, Genome Canada, Alberta Prion Research Institute, and Alberta Agriculture and Forestry through Genome Alberta. In

addition, MAL gratefully acknowledges the Canada Research Chair program and an NSERC Discovery grant.

Appendix A. Derivation of Eqs. (7) and (10)

We use $s_j(x,t), i_j(x,t)$ to represent the density of susceptible individuals and the density of infected individuals in group j, respectively, and use $h_j(x,t)$ to represent the prions in the environment shed from the infected individuals in group j. Then we consider the change of total susceptible individuals and infected individuals in group j due to direct and environmental transmission, and obtain the following equations:

$$\begin{aligned}\frac{d}{dt}\int_R s_j(x,t)dx =& -\beta\int_R s_j(x_j+\xi,t)\sum_k i_k(x_j+\xi,t)d\xi\\ &-\phi\int_R s_j(x_j+\xi,t)\sum_k h_k(x_j+\xi,t)d\xi,\end{aligned}\tag{A.1}$$

$$\begin{aligned}\frac{d}{dt}\int_R i_j(x,t)dx =&\beta\int_R s_j(x_j+\xi,t)\sum_k i_k(x_j+\xi,t)d\xi\\ &+\phi\int_R s_j(x_j+\xi,t)\sum_k h_k(x_j+\xi,t)d\xi.\end{aligned}\tag{A.2}$$

As we assume the distribution of individuals in each group is at its steady state and movement of individuals is fast, the density of susceptible individuals and the density of infected individuals in group j satisfy the following relations, at any given location x:

$$s_j(x,t) = S_j(t)u_j(x)N_j,\tag{A.3}$$

$$i_j(x,t) = I_j(t)u_j(x)N_j,\tag{A.4}$$

where $S_j(t)$ ($I_j(t)$, respectively) is the proportion of susceptible (infected, respectively) individuals in group j, and $S_j(t)+I_j(t)=1$.

To simplify the Eqs. (A.1) and (A.2), we still need to look at the rate of change of environmental hazard $h_j(x,t)$, which is affected by the shedding from the infected and its own degrading rate in the following:

$$\frac{\partial}{\partial t}h_j(x,t) = \alpha i_j(x,t) - \delta h_j(x,t),\tag{A.5}$$

where α is the rate at which prions are excreted by infected individuals, and δ is the rate at which prions are removed from environment. For any given x (fixed), we can solve $h_j(x,t)$ from the linear differential Eq. (A.5):

$$h_j(x,t) = N_j u_j(x)\left(\alpha\exp(-\delta t)\int_0^t I_j(\tau)\exp(\delta\tau)d\tau + \bar{h}_{j,0}(x)\right),\tag{A.6}$$

where the initial environmental hazard is

$$h_j(x,0) = h_{j,0}(x) = N_j u_j(x)\bar{h}_{j,0}(x),\tag{A.7}$$

This, again, enables us to separate spatial and temporal changes. So, $h_j(x,t)$ can be expressed in the following way:

$$h_j(x,t) = H_j(t)u_j(x)N_j,\tag{A.8}$$

where we define the prions shed per individual in group j at any given location x is

$$H_j(t) = \alpha\exp(-\delta t)\int_0^t I_j(\tau)\exp(\delta\tau)d\tau + \bar{h}_{j,0}(x).\tag{A.9}$$

We can now use Eqs. (A.3), (A.4) and (A.8) to simplify Eqs. (A.1), (A.2) and (A.5). For Eq. (A.1), we can simplify it as follows:

$$\begin{aligned}\frac{d}{dt}\int_R S_j(t)u_j(x)N_j dx =& -\beta\int_R S_j(t)u_j(x_j+\xi)N_j\sum_k I_k(t)u_k(x_j+\xi)N_k d\xi\\ &-\phi\int_R S_j(t)u_j(x_j+\xi)N_j\sum_k H_k(t)u_k(x_j+\xi)N_k d\xi,\end{aligned}\tag{A.10}$$

$$\begin{aligned}&\Rightarrow\ N_j\tfrac{d}{dt}S_j(t)\int_R u_j(x)dx\\ &=\ -\beta N_j S_j(t)\sum_k I_k(t)N_k\int_R u_j(x_j+\xi)u_k(x_j+\xi)d\xi\\ &\quad -\phi N_j S_j(t)\sum_k H_k(t)N_k\int_R u_j(x_j+\xi)u_k(x_j+\xi)d\xi,\end{aligned}\tag{A.11}$$

$$\begin{aligned}&\Rightarrow\ \tfrac{d}{dt}S_j(t)\\ &=\ -\beta S_j(t)\sum_k I_k(t)N_k\int_R u_j(x_j+\xi)u_k(x_j+\xi)d\xi\\ &\quad -\phi S_j(t)\sum_k H_k(t)N_k\int_R u_j(x_j+\xi)u_k(x_j+\xi)d\xi,\end{aligned}\tag{A.12}$$

$$\begin{aligned}&\Rightarrow\ \tfrac{d}{dt}S_j(t)\\ &=\ -S_j(t)\sum_k I_k(t)\beta_{jk}N_k - S_j(t)\sum_k H_k(t)\phi_{jk}N_k,\end{aligned}\tag{A.13}$$

where

$$\beta_{jk} = \beta\int_R u_j(\xi)u_k(\xi)d\xi,\tag{A.14}$$

$$\phi_{jk} = \phi\int_R u_j(\xi)u_k(\xi)d\xi,\tag{A.15}$$

are the effective pairwise direct and environmental, respectively, transmission rates between group j and group k, and both of them are constants given j and k. Similarly, we can simplify Eq. (A.2) to the following:

$$\frac{d}{dt}I_j(t) = S_j(t)\sum_k I_k(t)\beta_{jk}N_k + S_j(t)\sum_k H_k(t)\phi_{jk}N_k\tag{A.16}$$

$$= S_j(t)\left(\sum_k (I_k(t)\beta_{jk} + H_k(t)\phi_{jk})N_k\right).\tag{A.17}$$

Eq. (A.5) is simplified into

$$\frac{d}{dt}H_j(t) = \alpha I_j(t) - \delta H_j(t).\tag{A.18}$$

Now we obtain our model for one gender as follows:

$$\frac{d}{dt}S_j(t) = -S_j(t)\sum_k I_k(t)\beta_{jk}N_k - S_j(t)\sum_k H_k(t)\phi_{jk}N_k,\tag{A.19}$$

$$\frac{d}{dt}I_j(t) = S_j(t)\sum_k I_k(t)\beta_{jk}N_k + S_j(t)\sum_k H_k(t)\phi_{jk}N_k,\tag{A.20}$$

$$\frac{d}{dt}H_j(t) = \alpha I_j(t) - \delta H_j(t),\tag{A.21}$$

where

$$\beta_{jk} = \beta\mu_{jk},\tag{A.22}$$

$$\phi_{jk} = \phi\mu_{jk},\tag{A.23}$$

$$\mu_{jk} = \int_R u_j(\xi)u_k(\xi)d\xi,\tag{A.24}$$

where we call β_{jk} the coefficient of pairwise direct effective transmission, ϕ_{jk} the coefficient of pairwise environmental effective transmission, μ_{jk} the pairwise encounter rate. Transmission occurring in the same group can also be expressed in this way.

Appendix B. The trivial equilibrium is unstable in the homogeneous population

We want to show that the disease-free equilibrium, $(0,0,0,0)$, is unstable for the following system

$$\begin{bmatrix} I^f(t) \\ H^f(t) \\ I^m(t) \\ H^m(t) \end{bmatrix}' = W \begin{bmatrix} I^f(t) \\ H^f(t) \\ I^m(t) \\ H^m(t) \end{bmatrix}, \tag{B.1}$$

where $W = (w_{jk})$ is

$$\begin{bmatrix} N_f \sum_{k=-\infty}^{\infty} \beta^f_{jk} & N_f \sum_{k=-\infty}^{\infty} \phi^f_{jk} & N_m \sum_{q=-\infty}^{\infty} \beta^{fm}_{jq} & N_m \sum_{q=-\infty}^{\infty} \phi^{fm}_{jq} \\ \alpha & -\delta & 0 & 0 \\ N_f \sum_{k=-\infty}^{\infty} \beta^{mf}_{pk} & N_f \sum_{k=-\infty}^{\infty} \phi^{mf}_{pk} & N_m \sum_{q=-\infty}^{\infty} \beta^{m}_{pq} & N_m \sum_{q=-\infty}^{\infty} \phi^{m}_{pq} \\ 0 & 0 & \alpha & -\delta \end{bmatrix}, \tag{B.2}$$

with all the parameters being positive. We first simplify the system as follows

$$\vec{X}(t)' = W\vec{X}(t), \tag{B.3}$$

where

$$W = \begin{bmatrix} w_{11} & w_{12} & w_{13} & w_{14} \\ \alpha & -\delta & 0 & 0 \\ w_{31} & w_{32} & w_{33} & w_{34} \\ 0 & 0 & \alpha & -\delta \end{bmatrix}, \tag{B.4}$$

with

$w_{ij} > 0, \alpha > 0, \delta > 0.$

We want to show that the trivial equilibrium $\vec{X} = 0$ is unstable.

The solution to the system (B.3) can be written in the exponential form:

$$\vec{X}(t) = \exp(Wt)\vec{X}(0) \tag{B.5}$$

Note that all the off-diagonal elements of W are non-negative, so Wt is a Metzler (or, quasi-positive) matrix for $t > 0$ (see, e.g., Ngoc, 2006). According to the property of Metzler matrices (see Thieme et al., 2009, Theorem 2.4), the elements in the matrix $\exp(Wt)$ are positive.

The solution in Eq. (B.5) is a product of the matrix $\exp(Wt)$ and the non-negative vector $\vec{X}(0)$ with at least one positive element. Hence, $\vec{X}(t)$ is non-negative and has at least one positive element for $t > 0$. Without loss of generality, we assume $X_1(0) > 0$. Then, from (B.3), we know

$$X_1'(t) = \sum_i w_{1i}X_i(t) \geqslant w_{11}X_1(t) > 0 \tag{B.6}$$

because all the $X_i(t)$ are nonnegative and all the w_{1i}'s are positive. By Gronwall's Inequality (Gronwall, 1919), we obtain

$$X_1(t) \geqslant X_1(0)\exp(w_{11}t) \tag{B.7}$$

where $w_{11} > 0$. Therefore, $X_1(t)$ is bounded below by an exponentially growing quantity. Hence, the trivial equilibrium $\vec{X} = 0$ is unstable, that is, the spectral abscissa of W is positive.

Appendix C. Parameters from literature

Here, we list the source of parameter values for our numerical simulations (see Table C.1).

Table C.1
Parameter values from literature (MUDE for mule deer, and WTDE for white-tailed deer).

Parameter	Value/ range	Data & source (From Merrill et al., 2013 if not specified)
Density (deer/km^2)	0.5~10.5 /km * (mode: 2.2) * note: our current model is one dimensional.	Alberta 2007-2009, aerial survey: - MUDE: 0.79±2.12, range: 0-28.4; WTDE: 1.07±0.1, range: 0-22.9 Alberta Feb 2018, aerial survey: - MUDE: 2.4 (CFBW) 2.8(CGR) (Merrill et al., 2018) Saskatchewan, aerial survey: - MUDE: 0.67-2.72 (reported for WMZs 2000-2009); WTDE: 0.08-3.00 (reported for WMZs 1994-2009) (Saskatchewan Ministry of Environment, 2015)
Sex ratio (male: female)	0.05~0.80 (mode: 0.25)	Alberta, ground, 2006-2009: MUDE: Doe: Buck = 100: 9–21; WTDE: 100:1–19 Alberta, aerial, 2007: MUDE: Doe: Buck = 100: 43; WTDE: 100: 27 Saskatchewan, 1982-2017 (Western Association of Fish and Wildlife Agencies, 2018) - MUDE: long term average of buck: doe ratio: 100: 51, range: 0.38~0.63
Home range radius (km)	M: 3.58 km, F: 2.90 km (home range size: M: 8.6 km^2; F: 5.78 km^2)	Alberta deer home range size (km^2) - MUDE, female: summer: 6.74±5.41; winter: 4.81±2.67; - MUDE, male: summer: 12.65±4.23; winter: 4.55±1.18. - WTDE, female: summer: 4.82±4.53; winter: 4.70±3.02; - WTDE, male: summer: 10.09±7.49; winter: 6.39±3.86.
Group size of male (Combining this with sex ratio, the female group size is obtained.)	Male: 2 (Female: 2.5~40)	Alberta winter aerial survey 2006-2009: MUDE: 6.6±0.4; WTDE: 4.4±0.2. Alberta ground survey: Summer: MUDE: 1.8±1.2; WTDE: 1.5±0.8. Winter: MUDE: 5.4±0.3; WTDE: 4.4±1.2.
Basic direct transmission rate	0.032 yr^{-1}	(Miller et al., 2006) (Note: the range of the basic direct transmission rate has been increased based on the source)
Basic indirect transmission rate	0.787 mass^{-1}yr^{-1}	
Prion shedding rate	0.111 mass density^{-1} yr^{-1}	
Prion degeneration rate	2.55 yr^{-1}	

Appendix D. Simplification and convergence of series

In this appendix, we use the following formula for the geometric series and another basic series to simplify our series in Eqs. (94)-(98):

$$\sum_{k=1} r^k = \frac{r}{1-r}, \text{ for } |r| < 1 \tag{D.1}$$

$$\sum_{k=1} kr^k = \frac{r}{(1-r)^2}, \text{ for } |r| < 1. \tag{D.2}$$

In order to numerically obtain a minimum of c, we first need to make sure s is in a valid domain. In particular, we need to make sure the series in Eqs. (94)-(98) converges. Substituting expression (36) into Eq. (98), we simplify $J^m(s)$ as follows:

$$J^m(s) = \sum_{q\neq 0} c_1 \exp(-c_2\Delta x|q|)(\exp(-sq\Delta x) - 1) \tag{D.3}$$

$$= \frac{c_1\exp(-(c_2+s)\Delta x)}{1-\exp(-(c_2+s)\Delta x)} + \frac{c_1\exp(-(c_2-s)\Delta x)}{1-\exp(-(c_2-s)\Delta x)} - \frac{2c_1\exp(-c_2\Delta x)}{1-\exp(-c_2\Delta x)}. \tag{D.4}$$

We need $s < c_2$ for $J^m(s)$ to converge. For $L^f(s), L^m(s), L^{fm}(s)$ and $L^{mf}(s)$, recall the pairwise encounter rate between two females, between two males, between a female and a male:

$$\mu^f_{jk} = \frac{b_f}{4}(1 + b_f\Delta x|k-j|)\exp(-b_f\Delta x|k-j|), \tag{D.5}$$

$$\mu^m_{jk} = \frac{b_m}{4}(1 + b_m\Delta x|k-j|)\exp(-b_m\Delta x|k-j|), \tag{D.6}$$

$$\mu^{fm}_{jk} = \frac{b_f b_m(-b_f\exp(-b_m\Delta x|k-j|) + b_m\exp(-b_f\Delta x|k-j|))}{2(b_m+b_f)(b_m-b_f)} \tag{D.7}$$

$$\mu^{mf}_{kj} = \frac{b_m b_f(-b_m\exp(-b_f\Delta x|k-j|) + b_f\exp(-b_m\Delta x|k-j|))}{2(b_m+b_f)(b_f-b_m)} \tag{D.8}$$

$$= \mu^{fm}_{jk}. \tag{D.9}$$

We obtain the following simplified expressions:

$$L^f_j(s) = L^f(s) \tag{D.10}$$

$$= \frac{b_f}{4}\left[1 + \frac{(1+b_f\Delta x)\exp((b_f+s)\Delta x) - 1}{(\exp((b_f+s)\Delta x) - 1)^2} + \frac{(1+b_f\Delta x)\exp((b_f-s)\Delta x) - 1}{(\exp((b_f-s)\Delta x) - 1)^2}\right] \tag{D.11}$$

$$L_p^m(s) = L^m(s) \tag{D.12}$$

$$= \frac{b_m}{4}\left[1 + \frac{(1+b_m\Delta x)\exp((b_m+s)\Delta x) - 1}{(\exp((b_m+s)\Delta x) - 1)^2} + \frac{(1+b_m\Delta x)\exp((b_m-s)\Delta x) - 1}{(\exp((b_m-s)\Delta x) - 1)^2}\right] \tag{D.13}$$

$$L_j^{fm}(s) \tag{D.14}$$

$$= L^{fm}(s) \tag{D.15}$$

$$= \frac{b_f b_m}{2(b_m + b_f)} \tag{D.16}$$

$$+ \frac{b_f b_m}{2\left((b_m)^2 - (b_f)^2\right)}\left[\frac{b_m}{\exp((b_f+s)\Delta x) - 1} - \frac{b_f}{\exp((b_m+s)\Delta x) - 1}\right] \tag{D.17}$$

$$+ \frac{b_f b_m}{2\left((b_m)^2 - (b_f)^2\right)}\left[\frac{b_m}{\exp((b_f-s)\Delta x) - 1} - \frac{b_f}{\exp((b_m-s)\Delta x) - 1}\right] \tag{D.18}$$

$$L_p^{mf}(s) \tag{D.19}$$

$$= L^{mf}(s) \tag{D.20}$$

$$= \frac{b_m b_f}{2(b_f + b_m)} \tag{D.21}$$

$$+ \frac{b_m b_f}{2\left((b_f)^2 - (b_m)^2\right)}\left[\frac{b_f}{\exp((b_m+s)\Delta x) - 1} - \frac{b_m}{\exp((b_f+s)\Delta x) - 1}\right] \tag{D.22}$$

$$+ \frac{b_m b_f}{2\left((b_f)^2 - (b_m)^2\right)}\left[\frac{b_f}{\exp((b_m-s)\Delta x) - 1} - \frac{b_m}{\exp((b_f-s)\Delta x) - 1}\right] \tag{D.23}$$

$$= L^{fm}(s) \tag{D.24}$$

The condition for the convergence of the series is as follows: with the convergence range

$$0 < s < \min\{b_m, b_f, c_2\}. \tag{D.25}$$

Appendix E. An example of the numerical simulation of spreading speed

E.1. Input

See Table E.1 for a full list of input parameters for numerical simulations.

E.2. Calculating other parameters using inputs

- # of groups that consists of females in the simulating space $= F = \frac{space}{\Delta x} + 1 = \frac{450}{2} + 1 = 226 = M = \#$ of groups that consists of males in the simulating space, with group indices $0, 1, 2, 3, \cdots, 225$.
  Note: (i). We have assumed the same number of groups $F = M$ and the same home range center for group j of males and female, $x_j^f = x_j^m$. (ii). # of females in every female group is N_f, and # of groups that consists of females in the simulating space is F. (iii). F/space and M/space are also referred to as 'group density'.
- Home range center for each group: $x_j^f = x_j^m = j\Delta x$, $j = 0, 1, 2, \cdots, 225$, which are $0, 2, 4, 6, \cdots, 450$ in our case.
- Male dispersal matrix **E**. First, we set a value for c_1. Then e_{pq} is given in an expression of c_1, c_2, p, q (see Eq. (36)).
- Pairwise encounter rate: μ_{jk} is determined by $b_f, b^m, x_j^f, x_j^m, \Delta x, j, k$ (see Eqs. (D.5)-(D.8)).

E.3. Initial conditions

$$I_j^f(0) = \begin{cases} 1, & j = 0, 1, 2, 3 \\ 0, & j = 4, 5, 6, \cdots, 225 \end{cases} \tag{E.1}$$

$$I_j^m(0) = \begin{cases} 1, & j = 0, 1, 2, 3 \\ 0, & j = 4, 5, 6, \cdots, 225 \end{cases} \tag{E.2}$$

$$H_j^f(0) = 0, j = 0, 1, 2, \cdots, 225 \tag{E.3}$$

$$H_j^m(0) = 0, j = 0, 1, 2, \cdots, 225 \tag{E.4}$$

E.4. Solve ODE

Using Runge-Kutta (2,3) ('ode23' in Matlab), we solve the system (16)-(21) with initial conditions above. Note: $S_j^f(t) + I_j^f(t) = 1$ and $S_j^m(t) + I_j^m(t) = 1$ for any $t \geqslant 0$.

E.5. Find the time of reaching a threshold of infection

For every group, find the time t_j^f and t_j^m when $I_j^f(t)$ or $I_j^m(t)$ reaches a threshold. In our simulations, we set the threshold to 0.9999, so we look for the time of reaching 'almost full infection.' Other values could be used, but the spreading speed will be similar, because the shape of the traveling wave remains the same as it propagate along the domain (see Fig. 4).

E.6. Calculate the speed

Write time and location in pairs (t_j, x_j), where $t_j = \max\left(t_j^f, t_j^m\right)$, meaning that we use the time of the group reaching the threshold later for each location – recall that there are one group of males and one group of females for each home range center $x_j = x_j^f = x_j^m$.

Use the middle portion of points (see Fig. 9) to fit a straight line and get the slope, which is our goal – an approximation of the spreading spreed.

Table E.1
Input for numerical simulation of spreading speed.

N_f	group size of female	4
N_m	group size of male	2
Δx	distance between neighbouring group centers	2 km
-	space of simulation	450 km
β	the basic direct transmission rate	0.0326 yr^{-1}
ϕ	the basic environmental transmission rate	0.787 $mass^{-1}yr^{-1}$
α	the rate at which prions are excreted	0.111 yr^{-1}
δ	the degrading rate of prions from environment	2.55 yr^{-1}
c_1	determining the male dispersal rate	0.2
c_2	determining the male dispersal rate	0.2
b_f	determining the home range size of female	1.4979 km^2yr^{-1}
b_m	determining the home range size of male	1 km^2yr^{-1}

Appendix F. Mathematical calculation of spreading speed

A brief description of the mathematical calculation of spreading speed is as follows:

1. Input $\beta, \phi, N_f, N_m, \alpha, \delta, b_f, b_m, \Delta x, kRange, c_2$.

Note: (i) b_f, b_m determines the home ranges of female groups, and male groups. (ii) kRange is used to approximate infinite series by a truncated series. (iii) c_2 determines c_1, and therefore the dispersal rate for males. (iv) Relationships between input parameters can be incorporated here, e.g., the group size changes with the density (see Eq. (124)), instead of independent from each other.

2. Obtain the spreading speed $\min_s c(s)$ (see Eq. (118) and text above) for s in the convergence interval of all the series in the calculation (see Appendix D).

Appendix G. Eq. (12) is equivalent to a Kolmogorov backward equation

The dispersal equation from the main text is:

$$\frac{d}{dt}N_j(t) = \sum_{k=1,k\neq j}^{M} e_{jk}N_k - \sum_{k=1,k\neq j}^{M} e_{kj}N_j. \tag{G.1}$$

We rewrite it in order to match the order of terms in Sigman (2009, Chapter 9)

$$\frac{d}{dt}N_j(t) = -\sum_{k=1,k\neq j}^{M} e_{kj}N_j + \sum_{k=1,k\neq j}^{M} e_{jk}N_k. \tag{G.2}$$

$$= -\sum_{k=1,k\neq j}^{M} e_{kj}N_j + \sum_{k=1,k\neq j}^{M} e_{jk}N_k. \tag{G.3}$$

To simplify the derivation and match with the notation in Sigman's lecture note (Sigman 2009, Chapter 9), we let

$$\sum_{k=1,k\neq j}^{M} e_{kj} = a_j, \tag{G.4}$$

$$e_{jk} = a_j P_{kj}. \tag{G.5}$$

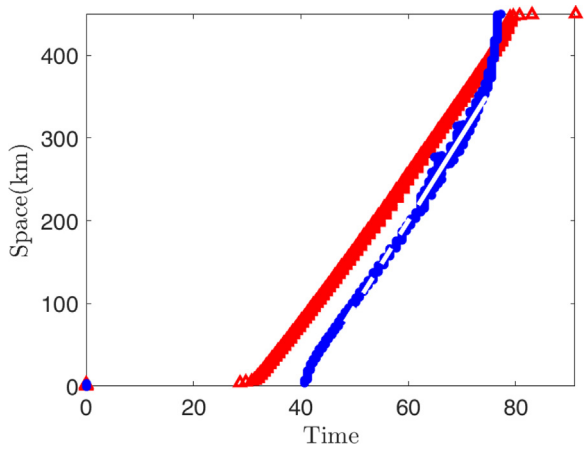

Fig. 9. The spatio-temporal spread of disease. Red triangles are for female groups, and blue stars are for male groups. For example, a red triangle placed at (x,y) means the infected fraction of the female group at location y reaches a threshold (in our case, we set the threshold to 99.99% – other thresholds can be used, but the computation of speed will not change much) at time x. Points along the dashed line are used to compute the spreading speed, which is the slope of the dashed line. Here, the spreading speed is approximately 10.3650 km/yr. Parameters are set to $\beta = 0.0326\,\mathrm{yr}^{-1}$, $\phi = 0.787\,\mathrm{mass}^{-1}\mathrm{yr}^{-1}$, $N_m = 2, N_f = 4$, $b_m = 1\,\mathrm{km}^2\mathrm{yr}^{-1}$, $b_f = 1.4979\,\mathrm{km}^2\mathrm{yr}^{-1}$, $c_2 = 0.2, \Delta x = 2\,\mathrm{km}$, $\alpha = 0.111\,\mathrm{yr}^{-1}$, $\delta = 2.55\,\mathrm{yr}^{-1}$.

Then, Eq. (G.1) is equivalent to

$$\frac{d}{dt}N_j(t) = -a_j N_j(t) + \sum_{k=1,k\neq j}^{M} a_j P_{kj} N_k(t). \tag{G.6}$$

Following Sigman's lecture note we use $\mathbf{P}(t) = \left(P_{ij}(t)\right)$ to denote the transition matrix, where $P_{ij}(t) = P(X(t) = j | X(0) = i)$, the initial state of an individual is $X(0)$, and the state at t is $X(t)$. Using $\mu_j(t)$ to denote the probability for an individual to be at state j, there are $N_j(t) = K\mu_j(t)$ individuals at state j at time t. The number of individuals at state j follows the relationship:

$$N_j(t) = \sum_{i=1}^{M} P_{ij}(t) N_i(0). \tag{G.7}$$

Substituting Eq. (G.7) into Eq. (G.6), we obtain an equation for $P_{ij}(t)$:

$$\begin{aligned} P'_{ij}(t) = & -a_j P_{ij}(t) + \sum_{k=1,k\neq j}^{M} a_j P_{kj} P_{ik}(t) \\ = & \begin{bmatrix} P_{i,1}(t) & P_{i,2}(t) & \cdots & P_{i,M}(t) \end{bmatrix} \begin{bmatrix} a_j P_{1,j} \\ a_j P_{2,j} \\ \cdots \\ -a_j \\ \cdots \\ a_j P_{M,j} \end{bmatrix}, \end{aligned}$$

which indicates that

$$\mathbf{P}(t)' = \mathbf{P}(t)\mathbf{Q}^T. \tag{G.8}$$

Therefore, we have

$$\left(\mathbf{P}(t)^T\right)' = \mathbf{Q}\mathbf{P}(t)^T, \tag{G.9}$$

which is in the form of a Kolmogorov backward equation for a CTMC. The transpose of our matrix defined in Eq. (13), $\mathbf{E}^T$, is the transition rate matrix $\mathbf{Q}$ for the CTMC.

Appendix H. Full general model in finite domain

Here we present a general model where the male groups can have different sizes. Because dispersal changes the male group size, it is better to track the numbers instead of proportions of hosts within a group so that we do not need an explicit group size. $\hat{S}^s_j(t)$ is the number of susceptible hosts in group j of sex s. $\hat{I}^s_j(t)$ is the number of infected hosts in group j of sex s. $\hat{H}^s_j(t)$ is the total concentration of prions shed by hosts in group j of sex s. Note that the dependent variables are not proportions of group compartments.

Assuming there are M male groups and F female groups, we obtain the full general model as:

$$\begin{aligned} \tfrac{d}{dt}\widehat{S}^f_j(t) = & -\widehat{S}^f_j(t)\sum_{k=1}^{F}\left(\widehat{I}^f_k(t)\beta^f_{jk} + \widehat{H}^f_k(t)\phi^f_{jk}\right) \\ & -\widehat{S}^f_j(t)\sum_{q=1}^{M}\left(\widehat{I}^m_q(t)\beta^{fm}_{jq} + \widehat{H}^m_q(t)\phi^{fm}_{jq}\right), \end{aligned} \tag{H.1}$$

$$\begin{aligned} \tfrac{d}{dt}\widehat{I}^f_j(t) = & \widehat{S}^f_j(t)\sum_{k=1}^{F}\left(\widehat{I}^f_k(t)\beta^f_{jk} + \widehat{H}^f_k(t)\phi^f_{jk}\right) \\ & +\widehat{S}^f_j(t)\sum_{q=1}^{M}\left(\widehat{I}^m_q(t)\beta^{fm}_{jq} + \widehat{H}^{fm}_q(t)\phi^{fm}_{jq}\right), \end{aligned} \tag{H.2}$$

$$\frac{d}{dt}\widehat{H}^f_j(t) = \alpha\widehat{I}^f_j(t) - \delta\widehat{H}^f_j(t), \tag{H.3}$$

$$\frac{d}{dt}\widehat{S}_p^m(t) = -\widehat{S}_p^m(t)\sum_{k=1}^{F}\left(\widehat{I}_k^f(t)\beta_{pk}^{mf} + \widehat{H}_k^f(t)\phi_{pk}^{mf}\right) - \widehat{S}_p^m(t)\sum_{q=1}^{M}\left(\widehat{I}_q^m(t)\beta_{pq}^{m} + \widehat{H}_q^m(t)\phi_{pq}^{m}\right) + \sum_{q\neq p} e_{pq}\widehat{S}_q^m(t) - \widehat{S}_p^m(t)\sum_{q\neq p} e_{qp}, \tag{H.4}$$

$$\frac{d}{dt}\widehat{I}_p^m(t) = \widehat{S}_p^m(t)\sum_{k=1}^{F}\left(\widehat{I}_k^f(t)\beta_{pk}^{mf} + \widehat{H}_k^f(t)\phi_{pk}^{mf}\right) + \widehat{S}_p^m(t)\sum_{q=1}^{M}\left(\widehat{I}_q^m(t)\beta_{pq}^{m} + \widehat{H}_q^m(t)\phi_{pq}^{m}\right) + \sum_{q\neq p} e_{pq}\widehat{I}_q^m(t) - \widehat{I}_p^m(t)\sum_{q\neq p} e_{qp}, \tag{H.5}$$

$$\frac{d}{dt}\widehat{H}_p^m(t) = \alpha\widehat{I}_p^m(t) - \delta\widehat{H}_p^m(t), \tag{H.6}$$

where superscripts f and m on variables denote the sex as described in Table 1,

$$j = 1, 2, \cdots, F, \tag{H.7}$$

$$p = 1, 2, \cdots, M, \tag{H.8}$$

$$\beta_{jq}^{fm} = \beta\mu_{jq}^{fm}, \tag{H.9}$$

$$\phi_{jq}^{fm} = \phi\mu_{jq}^{fm}, \tag{H.10}$$

$$\mu_{jq}^{fm} = \int_R u_j^f(\xi)u_q^m(\xi)d\xi, \tag{H.11}$$

$$\beta_{pk}^{mf} = \beta\mu_{pk}^{mf}, \tag{H.12}$$

$$\phi_{pk}^{mf} = \phi\mu_{pk}^{mf}, \tag{H.13}$$

$$\mu_{pk}^{mf} = \int_R u_p^m(\xi)u_k^f(\xi)d\xi, \tag{H.14}$$

$$\beta_{jk}^{s} = \beta\mu_{jk}^{s}, \tag{H.15}$$

$$\phi_{jk}^{s} = \phi\mu_{jk}^{s}, \tag{H.16}$$

$$\mu_{jk}^{s} = \int_R u_j^s(\xi)u_k^s(\xi)d\xi, \tag{H.17}$$

$$s = f, m. \tag{H.18}$$

with initial conditions:

$$\hat{S}_j^f(0) = \hat{S}_{j,0}^f, \hat{I}_j^f(0) = \hat{I}_{j,0}^f, \hat{H}_j^f(0) = \hat{H}_{j,0}^f, \text{ for } j = 1, 2, \cdots, F, \tag{H.19}$$

$$\hat{S}_p^m(0) = \hat{S}_{p,0}^m, \hat{I}_p^m(0) = \hat{I}_{p,0}^m, \hat{H}_p^m(0) = \hat{H}_{p,0}^m, \text{ for } p = 1, 2, \cdots, M. \tag{H.20}$$

For the male dispersal rate e_{qp}, we assume an exponentially decreasing rate function

$$e_{qp} = e_{pq} = c_1\exp(-c_2\Delta x|p-q|), \tag{H.21}$$

where c_1 denotes the magnitude and c_2 denotes the drop off with distance.

Appendix I. Derivation of Eqs. (60)–(62)

The idea is to consider the relative value of x compared with x_j and x_k, and separate the 1D space into three intervals. Without loss of generalization, we first assume $x_j < x_k$.

$$\mu_{jk}^f = \int_R u_j^f(x)u_k^f(x)dx \tag{I.1}$$

$$= \int_R \frac{b_f}{2}\exp(-b_f|x-x_j|)\frac{b_f}{2}\exp(-b_f|x-x_k|)dx \tag{I.2}$$

$$= \frac{b_f^2}{4}\int_R \exp(-b_f(|x-x_j| + |x-x_k|))dx \tag{I.3}$$

$$= \frac{b_f^2}{4}\int_{-\infty}^{x_j}\exp(-b_f(-x+x_j-x+x_k))dx \tag{I.4}$$

$$+ \frac{b_f^2}{4}\int_{x_j}^{x_k}\exp(-b_f(x_k-x_j))dx \tag{I.5}$$

$$+ \frac{b_f^2}{4}\int_{x_k}^{\infty}\exp(-b_f(x-x_j+x-x_k))dx \tag{I.6}$$

$$= \frac{b_f^2}{4}\int_{-\infty}^{x_j}\exp(-b_f(-2x+x_j+x_k))dx \tag{I.7}$$

$$+ \frac{b_f^2}{4}\int_{x_j}^{x_k}\exp(-b_f(x_k-x_j))dx \tag{I.8}$$

$$+ \frac{b_f^2}{4}\int_{x_k}^{\infty}\exp(-b_f(2x-x_j-x_k))dx \tag{I.9}$$

$$= \frac{b_f^2}{4}\frac{1}{2b_f}\exp(-b_f(x_k-x_j)) \tag{I.10}$$

$$+ \frac{b_f^2}{4}(x_k-x_j)\exp(-b_f(x_k-x_j)) \tag{I.11}$$

$$+ \frac{b_f^2}{4}\frac{1}{-2b_f}(-\exp(-b_f(x_k-x_j))) \tag{I.12}$$

$$= \frac{b_f}{4}\exp(-b_f(x_k-x_j)) \tag{I.13}$$

$$+ \frac{b_f^2}{4}(x_k-x_j)\exp(-b_f(x_k-x_j)) \tag{I.14}$$

$$= \frac{b_f}{4}(1+b_f(x_k-x_j))\exp(-b_f(x_k-x_j)) \tag{I.15}$$

$$= \frac{b_f}{4}(1+b_f\Delta x|k-j|)\exp(-b_f\Delta x|k-j|). \tag{I.16}$$

For $x_k < x_j$, we can obtain

$$\mu_{jk}^f = \frac{b_f}{4}(1+b_f(x_j-x_k))\exp(-b_f(x_j-x_k)). \tag{I.17}$$

Combining those two cases, we obtain

$$\mu_{jk}^f = \frac{b_f}{4}(1+b_f|x_k-x_j|)\exp(-b_f|x_k-x_j) \tag{I.18}$$

For special evenly-spaced home ranges, $x_j = j*\Delta x$, we can obtain

$$\mu_{jk}^f = \frac{b_f}{4}(1+b_f\Delta x|k-j|)\exp(-b_f\Delta x|k-j|), \tag{I.19}$$

which is Eq. (60) for females. The equation for males can be obtained by replacing b_f with b_m.

We use a similar to calculate μ_{jk}^{fm}. Note that $b_f - b_m$ can not be the denominator when $b_f = b_m$. That is how we got two separate cases.

Appendix J. A simplified explanation for edge density

In landscape ecology, edges are defined as the boundaries of different habitat types, and edge density equals the edge length per unit area (see, e.g. Turner and Gardner, 2015). As an simple example, we assume there are two landscape types (denoted by white and green) in a squared region (3 km by 3 km) (Fig. 10). If there

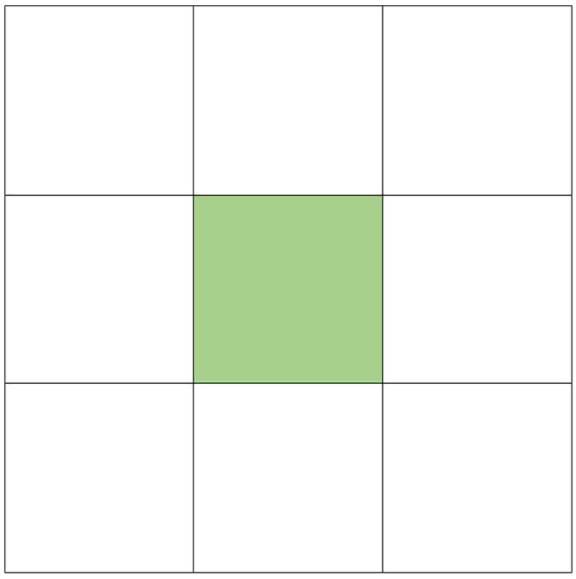

Fig. 10. A region with two landscape types.

are forest in the middle (1 km by 1 km) of the region surrounded by grassland. Then, the edge density in this region is 4/9 km/km^2.

References

Adams, H.L., Kissell, R.E., Ratajczak, D., Warr, E.L., Applegate, R.D., Barrett, L., Lavacot, T., Graves, D., 2020. Relationships among white-tailed deer density, harvest, and landscape metrics in TN, USA. Eur. J. Wildl. Res. 66 (1), 19.

Altendorf, K.B., Laundré, J.W., López González, C.A., Brown, J.S., 2001. Assessing effects of predation risk on foraging behavior of mule deer. J. Mammalogy 82 (2), 430–439.

Auger-Méthé, M., Lewis, M.A., Derocher, A.E., 2016. Home ranges in moving habitats: polar bears and sea ice. Ecography 39 (1), 26–35.

Bartmann, R.M., White, G.C., Carpenter, L.H., 1992. Compensatory mortality in a Colorado mule deer population. Wildlife Monographs, 3–39.

Belsare, A.V., Gompper, M.E., Keller, B., Sumners, J., Hansen, L., Millspaugh, J.J., 2020. An agent-based framework for improving wildlife disease surveillance: A case study of chronic wasting disease in Missouri white-tailed deer. Ecol. Model. 417, 108919.

Briscoe, B.K., Lewis, M.A., Parrish, S.E., 2002. Home range formation in wolves due to scent marking. Bull. Math. Biol. 64 (2), 261–284.

Cook, J.G., Irwin, L.L., Bryant, L.D., Riggs, R.A., Thomas, J.W., 2004. Thermal cover needs of large ungulates: a review of hypothesis tests, in: Transactions of the 69th North American Wildlife and Natural Resources Conference: 708–726, 708–726, 2004.

DeVivo, M.T., Edmunds, D.R., Kauffman, M.J., Schumaker, B.A., Binfet, J., Kreeger, T.J., Richards, B.J., Schätzl, H.M., Cornish, T.E., 2017. Endemic chronic wasting disease causes mule deer population decline in Wyoming. PLoS ONE 12, (10) e0186512.

DeYoung, C.A., 2011. Population Dynamics, in: D.G. Hewitt (Ed.), Biology and Management of White-tailed Deer, chap. 5, CRC Press, 147–180.

Edmunds, D.R., Kauffman, M.J., Schumaker, B.A., Lindzey, F.G., Cook, W.E., Kreeger, T.J., Grogan, R.G., Cornish, T.E., 2016. Chronic wasting disease drives population decline of white-tailed deer. PLoS ONE 11, (8) e0161127.

Escobar, L.E., Pritzkow, S., Winter, S.N., Grear, D.A., Kirchgessner, M.S., Dominguez-Villegas, E., Machado, G., Townsend Peterson, A., Soto, C., 2020. The ecology of chronic wasting disease in wildlife. Biol. Rev. 95 (2), 393–408.

Freddy, D., 1985. Quantifying capacity of winter ranges to support deer–evaluation of thermal cover used by deer, Wildlife Research Report. Colorado Division of Wildlife, Denver, Colorado, pp. 13–36.

Garlick, M.J., Powell, J.A., Hooten, M.B., MacFarlane, L.R., 2014. Homogenization, sex, and differential motility predict spread of chronic wasting disease in mule deer in southern Utah. J. Math. Biol. 69 (2), 369–399.

Gronwall, T.H., 1919. Note on the derivatives with respect to a parameter of the solutions of a system of differential equations. Ann. Math., 292–296

Habib, T.J., Merrill, E.H., Pybus, M.J., Coltman, D.W., 2011. Modelling landscape effects on density–contact rate relationships of deer in eastern Alberta: implications for chronic wasting disease. Ecol. Model. 222 (15), 2722–2732.

Hamelin, F.M., Lewis, M.A., 2010. A differential game theoretical analysis of mechanistic models for territoriality. J. Math. Biol. 61 (5), 665–694.

EFSA BIOHAZ Panel (EFSA Panel on Biological Hazards), Ricci, A., Allende, A., Bolton, D., Chemaly, M., Davies, R., Fernández Escámez, P.S., Gironés, R., Herman, L., Koutsoumanis, K., Lindqvist, R., Nørrung, B., Robertson, L., Sanaa, M., Skandamis, P., Snary, E., Speybroeck, N., Kuile, B.T., Threlfall, J., Wahlström, H., Benestad, S., Gavier-Widen, D., Miller, M.W., Ru, G., Telling, G.C., Tryland, M., Ortiz Pelaez, A., Simmons, M., 2017, Scientific opinion on chronic wasting disease (CWD) in cervids, EFSA Journal 15 (1), ISSN 18314732.

Hammond, R.A., 2015. Considerations and best practices in agent-based modeling to inform policy, in: Assessing the Use of Agent-Based Models for Tobacco Regulation, National Academies Press (US), 161–194.

Hefley, T.J., Hooten, M.B., Russell, R.E., Walsh, D.P., Powell, J.A., 2017. When mechanism matters: Bayesian forecasting using models of ecological diffusion. Ecol. Lett. 20 (5), 640–650.

Hinrichsen, D., Son, N., 1998. μ-Analysis and robust stability of positive linear systems. Appl. Math. Computer Sci. 8 (2), 253–268.

Holgate, P., 1971. Random walk models for animal behavior, in: G.P. Patil, E. Pielou, W.E. Waters (Eds.), Sampling and Modeling Biological Populations and Population Dynamics, vol. 2, chap. 1, Pen State University Press, University Park, Pennsylvania, USA, 1–12, 1971.

Horn, R.A., Johnson, C.R., 2012. Matrix Analysis. Cambridge University Press.

Kie, J.G., Bowyer, R.T., Nicholson, M.C., Boroski, B.B., Loft, E.R., 2002. Landscape heterogeneity at differing scales: effects on spatial distribution of mule deer. Ecology 83 (2), 530–544.

Kot, M., Lewis, M.A., van den Driessche, P., 1996. Dispersal data and the spread of invading organisms. Ecology 77 (7), 2027–2042.

Lee, J., Hillen, T., Lewis, M., 2008. Continuous traveling waves for prey-taxis. Bull. Math. Biol. 70 (3), 654–676.

Lewis, M.A., Murray, J.D., 1993. Modelling territoriality and wolf–deer interactions. Nature 366 (6457), 738–740.

Lewis, M.A., White, K.A.J., Murray, J.D., 1997. Analysis of a model for wolf territories. J. Math. Biol. 35 (7), 749–774.

Lewis, M., Rencławowicz, J., van den Driessche, P., 2006. Traveling waves and spread rates for a West Nile virus model. Bull. Math. Biol. 68 (1), 3–23.

Lewis, M.A., Petrovskii, S.V., Potts, J.R., 2016. The Mathematics Behind Biological Invasions, vol. 44. Springer.

Lewis, M.A., Marculis, N.G., Shen, Z., 2018. Integrodifference equations in the presence of climate change: persistence criterion, travelling waves and inside dynamics. J. Math. Biol. 77 (6), 1649–1687.

Lin, J., Andreasen, V., Casagrandi, R., Levin, S.A., 2003. Traveling waves in a model of influenza A drift. J. Theoretical Biology 222 (4), 437–445.

Long, E.S., Diefenbach, D.R., Rosenberry, C.S., Wallingford, B.D., Grund, M.D., 2005. Forest cover influences dispersal distance of white-tailed deer. J. Mammal. 86 (3), 623–629.

Maidana, N.A., Yang, H.M., 2008. Describing the geographic spread of dengue disease by traveling waves. Math. Biosci. 215 (1), 64–77.

Martinez-Garcia, R., Fleming, C.H., Seppelt, R., Fagan, W.F., Calabrese, J.M., 2020. How range residency and long-range perception change encounter rates. J. Theor. Biol. 110267.

Massé, A., Côté, S.D., 2009. Habitat selection of a large herbivore at high density and without predation: trade-off between forage and cover? J. Mammal. 90 (4), 961–970.

Mathiason, C.K., Powers, J.G., Dahmes, S.J., Osborn, D.A., Miller, K.V., Warren, R.J., Mason, G.L., Hays, S.A., Hayes-Klug, J., Seelig, D.M., et al., 2006. Infectious prions in the saliva and blood of deer with chronic wasting disease. Science 314 (5796), 133–136.

Mathiason, C.K., Hays, S.A., Powers, J., Hayes-Klug, J., Langenberg, J., Dahmes, S.J., Osborn, D.A., Miller, K.V., Warren, R.J., Mason, G.L., et al., 2009. Infectious prions in pre-clinical deer and transmission of chronic wasting disease solely by environmental exposure. PLoS ONE 4, (6) e5916.

Mejia Salazar, M.F., et al., 2017. Social dynamics among mule deer and how they visit various environmental areas: implications for chronic wasting disease transmission, Ph.D. thesis, University of Saskatchewan, 2017.

Merrill, E.H., Habib, T., Nobert, B., Brownrigg, E., Jones, P., Garrett, C., et al., 2011. Alberta Chronic Wasting Disease: North Border Deer Study, Final Report, unpublished. Edmonton: University of Alberta.

Meyer, C.D., 2000. Matrix Analysis and Applied Linear. Algebra vol. 71, Siam.

Michael, W.M., 2001. Chronic wasting disease in mule deer: disease dynamics and control. Journal of Wildlife Management 65 (2), 205–215.

Moll, R.J., McRoberts, J.T., Millspaugh, J.J., Wiskirchen, K.H., Sumners, J.A., Isabelle, J.L., Keller, B.J., Montgomery, R.A., 2021. A rare 300 kilometer dispersal by an adult male white-tailed deer, Ecology and Evolution.

Monello, R.J., Powers, J.G., Hobbs, N.T., Spraker, T.R., Watry, M.K., Wild, M.A., 2014. Survival and population growth of a free-ranging elk population with a long history of exposure to chronic wasting disease. J. Wildl. Manag. 78 (2), 214–223.

Moorcroft, P.R., 1997. Territoriality and carnivore home ranges, Ph.D. thesis, Princeton University.

Moorcroft, P.R., Lewis, M.A., Crabtree, R.L., 1999. Home range analysis using a mechanistic home range model. Ecology 80 (5), 1656–1665.

Moorcroft, P.R., Lewis, M.A., Crabtree, R.L., 2006. Mechanistic home range models capture spatial patterns and dynamics of coyote territories in Yellowstone. Proc. R. Soc. B: Biological Sci. 273 (1594), 1651–1659.

Moorcroft, P.R., Moorcroft, P., Lewis, M.A., 2006. Mechanistic Home Range Analysis. Princeton University Press.

Mysterud, A., Rolandsen, C.M., 2018. A reindeer cull to prevent chronic wasting disease in Europe. Nature Ecol. Evol. 2 (9), 1343–1345.
Ngoc, P.H.A., 2006. A Perron-Frobenius theorem for a class of positive quasi-polynomial matrices. Appl. Math. Letters 19 (8), 747–751.
Nixon, C.M., Mankin, P.C., Etter, D.R., Hansen, L.P., Brewer, P.A., Chelsvig, J.E., Esker, T.L., Sullivan, J.B., 2007. White-tailed deer dispersal behavior in an agricultural environment. Am. Midland Naturalist 157 (1), 212–220.
Nobert, B.R., Merrill, E.H., Pybus, M.J., Bollinger, T.K., Hwang, Y.T., 2016. Landscape connectivity predicts chronic wasting disease risk in Canada. J. Appl. Ecol. 53 (5), 1450–1459.
O'Hara Ruiz, M., Kelly, A.C., Brown, W.M., Novakofski, J.E., Mateus-Pinilla, N.E., 2013. Influence of landscape factors and management decisions on spatial and temporal patterns of the transmission of chronic wasting disease in white-tailed deer. Geospatial Health 8 (1), 215–227.
Pishro-Nik, H., 2016. Introduction to Probability, Statistics, and Random Processes. Kappa Research, LLC.
Plante, M., Lowell, K., Potvin, F., Boots, B., Fortin, M.-J., 2004. Studying deer habitat on Anticosti Island, Québec: relating animal occurrences and forest map information. Ecol. Model. 174 (4), 387–399.
Potapov, A., Merrill, E.H., Lewis, M.A., 2012. Wildlife disease elimination and density dependence. Proc. R. Soc. B: Biolog. Sci. 279 (1741), 3139–3145.
Potapov, A., Merrill, E.H., Pybus, M., Coltman, D., Lewis, M.A., 2013. Chronic wasting disease: Possible transmission mechanisms in deer. Ecol. Model. 250, 244–257.
Potapov, A., Merrill, E.H., Pybus, M., Lewis, M.A., 2016. Chronic wasting disease: Transmission mechanisms and the possibility of harvest management. PLoS ONE 11, (3) e0151039.
Reluga, T.C., Medlock, J., Galvani, A.P., 2006. A model of spatial epidemic spread when individuals move within overlapping home ranges. Bull. Math. Biol. 68 (2), 401–416.
Rivera, N.A., Brandt, A.L., Novakofski, J.E., Mateus-Pinilla, N.E., 2019. Chronic wasting disease in cervids: Prevalence, impact and management strategies. Veterinary Medicine: Research and Reports 10, 123.
Robinson, S.J., Samuel, M.D., Rolley, R.E., Shelton, P., 2013. Using landscape epidemiological models to understand the distribution of chronic wasting disease in the Midwestern USA. Landscape Ecol. 28 (10), 1923–1935.
Saltelli, A., Tarantola, S., Campolongo, F., Ratto, M., 2004. Sensitivity Analysis in Practice: a Guide to Assessing Scientific Models, vol. 1. Wiley Online Library.
Samuel, M.D., Storm, D.J., 2016. Chronic wasting disease in white-tailed deer: Infection, mortality, and implications for heterogeneous transmission, Ecology 97 (11) (2016) 3195–3205, ISSN 00129658.
Schauber, E.M., Storm, D.J., Nielsen, C.K., 2007. Effects of joint space use and group membership on contact rates among white-tailed deer. J. Wildl. Manag. 71 (1), 155–163.
Sigman, K., 2009. Lecture Notes on Stochastic Modeling I, URL:http://www.columbia.edu/ ks20/stochastic-I/stochastic-I.html, 2009.
Skelton, N.K., 2010. Migration, dispersal, and survival patterns of mule deer (Odocoileus hemionus) in a chronic wasting disease-endemic area of southern Saskatchewan, Ph.D. thesis, University of Saskatchewan.
Skuldt, L.H., Mathews, N.E., Oyer, A.M., 2008. White-tailed deer movements in a chronic wasting disease area in south-central Wisconsin. J. Wildl. Manag. 72 (5), 1156–1160.
Storm, D.J., Samuel, M.D., Rolley, R.E., Shelton, P., Keuler, N.S., Richards, B.J., Van Deelen, T.R., 2013. Deer density and disease prevalence influence transmission of chronic wasting disease in white-tailed deer. Ecosphere 4 (1), 1–14.
Thieme, H.R., 2009. Spectral bound and reproduction number for infinite-dimensional population structure and time heterogeneity. SIAM J. Appl. Math. 70 (1), 188–211.
Uehlinger, F., Johnston, A., Bollinger, T., Waldner, C., 2016. Systematic review of management strategies to control chronic wasting disease in wild deer populations in North America. BMC Veterinary Res. 12 (1), 173.
Walter, W., Beringer, J., Hansen, L., Fischer, J., Millspaugh, J., Vercauteren, K., 2011. Factors affecting space use overlap by white-tailed deer in an urban landscape. Int. J. Geographical Inform. Sci. 25 (3), 379–392.
Walter, W.D., Evans, T.S., Stainbrook, D., Wallingford, B.D., Rosenberry, C.S., Diefenbach, D.R., 2018. Heterogeneity of a landscape influences size of home range in a North American cervid. Sci. Rep. 8 (1), 1–9.
Williams, E., 2005. Chronic wasting disease. Vet. Pathol. 42 (5), 530–549.
Williams, E.S., Miller, M.W., Kreeger, T.J., Kahn, R.H., Thorne, E.T., 2002. Chronic wasting disease of deer and elk: a review with recommendations for management. J. Wildl. Manag., 551–563
Zhang, K.F., Zhao, X.-Q., 2007. Spreading speed and travelling waves for a spatially discrete SIS epidemic model. Nonlinearity 21 (1), 97.
Turner, M.G., Gardner, R.H., 2015. Landscape ecology in theory and practice.